Institute for Integrated Signal Processing Systems (ISS)
RWTH Aachen University
Prof. Dr.-Ing. Gerd Ascheid

Student Research Project S 295

Opportunistic Beamforming in Multiuser MIMO Systems with an Application to HSDPA

by

Erdem Koç

Matr.-No. 253346

October

Support by :
Prof. Dr.-Ing. Gerd Ascheid
Dipl.-Ing. Markus Jordan

I assure that this project was accomplished by me, without any foreign assistance except the official support of the chair. The used literature is fully indicated in the bibliography.

Aachen, 05.10.2005

(Erdem Koç)

Contents

1 Motivation

The first 3G networks are developed according to a 3GPP standard version called Release 99. Release 99 has a lot of improvements compared to 2G and 2.5G networks like GSM and EDGE. But still it should be considered that the maximum data rate per user in a Release 99 system is 384kbit/s, while 2.5G systems can reach values higher than 100kbit/s. These can be considered as comparable values and may decrease the interest in Release 99. HSDPA is a very important 3G technology that comes into play at this point. It offers a theoretical maximum data rate of 14400 kbit/s which is a very huge improvement. HSDPA aims to improve downlink capacity. The idea behind this is that, unlike the symmetric use of sources in voice communications 3G mobile systems make applications like web browsing and video streaming possible. These applications are highly asymmetrical from downlink and up-link point of view and make downlink improvement more interesting than up-link. [1] HSDPA is still subject to optimization. HSDPA scheduler technology makes it possible to exploit a different diversity technique called *multiuser diversity*. Multiuser diversity results from the fact that different users experience different channel dynamics. However, in a practical wireless system like HSDPA, multiuser diversity may be limited by slow variation of the channel or a strong line of sight component in the Ricean channel model. *Opportunistic Beamforming* [1] is a technique to increase the system throughput in scenarios where the natural dynamics of the channel do not allow multiuser diversity to be fully exploited. In scenarios like these, quality of service (QoS) constraints prohibit scheduling of users in their channel peaks because waiting for the next peak may not be feasible from QoS point of view. Here, increasing the natural dynamics of the channel with artificially induced fading can be a useful solution. This idea was investigated in the literature for MISO systems. For example in [1], a scheme to randomize the transmit powers and phases resulting in faster channel fading was proposed.

In parallel to this, MIMO systems are increasingly being considered to improve the performance of a wireless system. Wireless MIMO technology can significantly increase the data rate by exploiting the extra degrees of freedom afforded by the multiple antennas at both transmitter and receiver [2]. This fact makes application of MIMO systems to current wireless technology interesting. And a combination of the opportunistic beamforming to increase the channel dynamics and MIMO communication to exploit extra degrees of freedom can be considered to improve the system throughput even more. In [2] and [3] some algorithms to apply this idea were proposed. How much gain this combination of MIMO structure and opportunistic beamforming may bring under realistic conditions like feedback delay, limited number of antennas and antenna spacing, multipath interference, intercell interference etc. is still an area that has to be investigated in more detail. Especially feedback delay stays as an important limiting factor on the performance of opportunistic beanforming, because up-to-date channel information is very crucial for the performance of systems that use feedback information coming from the mobile stations and increasing channel dynamics via opportunistic beamforming decreases the reliability of this feedback information. To decrease the effect of this feedback delay problem adaptive filtering can be used. Considering the affordable computational power, an estimator that will try to estimate the current channel quality from the delayed version of the channel feedback information can be considered to bring an improvement to the system performance that suffers from feedback delay.

[1] It should be noted that there is also a corresponding up-link enhancement called HSUPA.

Outline

Chapter 1 gives a short introduction to the objective of this work. Chapter 2 explains some fundamentals and gives some derivations about multiuser diversity, estimation filters, opportunistic beamforming, MIMO systems, extension of opportunistic beamforming to MIMO systems and an overview of UMTS/HSDPA. Chapter 3 gives the details of the scenario that is used in the simulations. Chapter 4 presents and discusses the results of simulations. Chapter 5 draws the main conclusions of this work.

2 Fundamentals

2.1 Multiuser Diversity and Opportunistic Beamforming on MISO Systems

Due to constructive and destructive interference of multipaths, a wireless channel experiences fading. This phenomenon has to be taken care of in order to communicate through the wireless channel and several different diversity techniques are possible to cope with fading. Apart from time, frequency and space diversity techniques that are widely used, another diversity technique called ”multiuser diversity” has became popular to increase performance of multiuser systems. However, multiuser diversity is different with respect to other diversity techniques. It is a system level diversity technique that approaches fading issue from a different point of view.

In [4] it is shown that, in a multiuser system in order to increase the system capacity it is optimal to schedule only the user with the best channel condition at that particular time. When this rule is applied multiuser diversity gain follows, because at any time among many users with independent channel fading, there is one user who is likely to have a very good channel condition which can be exploited by the system.

This means that, from multiuser diversity point of view increased channel dynamics may be desirable to increase the possibility of finding a user with a very good channel condition at a particular time. This is actually the point where opportunistic beamforming comes into consideration. Because, channel fading itself may not be enough to obtain necessary channel dynamics especially when there is a line-of-sight path and/or little scattering between the sender and the receiver.

Note that if the exact phase and magnitude of the channel of a specific user in the cell was known, beamforming could be done accordingly to increase SNR. But this would require excessive amount of feedback information from each user and also a lot of computational power. Opportunistic beamforming approaches the problem in a randomized fashion and aims to increase the probability of a user being in or close to the beamforming configuration.

In [1] it is shown that opportunistic beamforming asymptotically approaches to coherent beamforming and the speed of approach is inversely proportional to the number of antennas at the transmitter side.

One of the another big advantages of opportunistic beamforming is the implementation cost to existing systems. From the receiver point of view it is completely invisible and for the transmitter side it requires only an antenna array that will introduce necessary amount of channel dynamics.

In the following subsections, *multiuser diversity*, *opportunistic beamforming* and *proportional fair scheduling* are analysed in more detail.

2.1.1 Multiuser Diversity

In [5], the sum capacity of the downlink of a multiuser system is given as:

$$C_{sum} = \mathbb{E}\left[\log\left(1 + \frac{P^*(\overline{h})(max_{k=1...K}|h_k^2|)}{N_0}\right)\right] \tag{2.1}$$

where $P^*(\overline{h})$ is power allocation term coming from water filling solution and is defined according to the system structure. In order to explain multiuser diversity mathematically the term that should be focused on is $max_{k=1...K}|h_k^2|$ which is the reason of multiuser diversity gain. To be more specific, define

$$|h|^2 := max_{k=1...K}|h_k|^2 \tag{2.2}$$

where $h_1, h_2, ..., h_K$ are i.i.d. $\mathcal{CN}(0,1)$ random variables (Rayleigh). It can be shown that

$$\mathbb{E}\left[|h|^2\right] = \sum_{k=1}^{K} \frac{1}{k} \tag{2.3}$$

and from 2.3 it follows that

$$\frac{\mathbb{E}\left[|h|^2\right]}{\log_e K} \to 1 \qquad \text{as} \qquad K \to \infty$$

thus *the mean of the effective channel power grows logarithmically with the number of users*. Now furthermore a line-of-sight component can be assumed and hence the random variables $h_1, h_2, ..., h_K$ are this time i.i.d. $\mathcal{CN}(\sqrt{\kappa}/\sqrt{1+\kappa}, 1/(1+\kappa))$ (Ricean). In this case the relation above becomes

$$\frac{\mathbb{E}\left[|h|^2\right]}{\log_e K} \to \frac{1}{1+\kappa} \qquad \text{as} \qquad K \to \infty$$

that is, the mean of the effective channel is now reduced by a factor $1+\kappa$ compared to Rayleigh fading case. In the light of the above derivations effect of multiuser diversity can be seen in figure 2.1

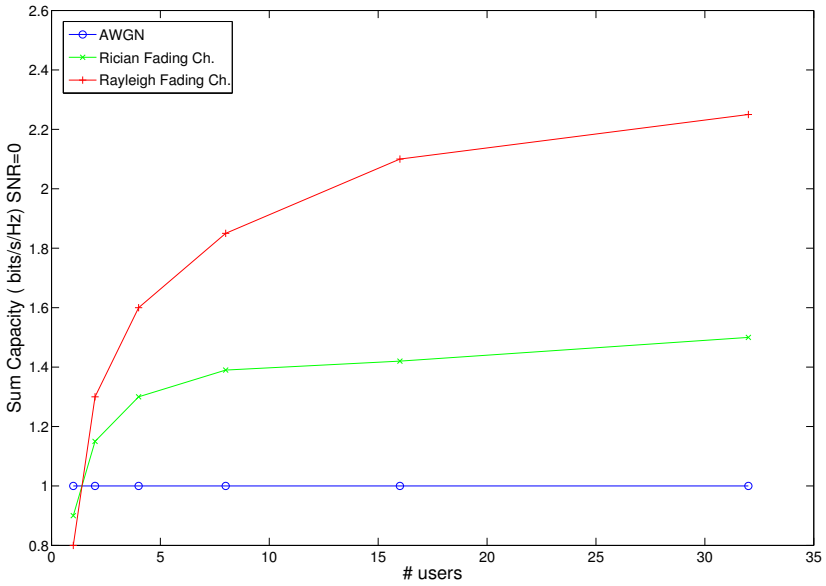

Figure 2.1: Multiuser diversity gain for Rayleigh and Ricean fading channels.

2.1.2 Proportional Fair Scheduling

The idea of scheduling the user with the best channel condition at a particular time is already shown to improve the overall system throughput. However, in a practical wireless multiuser system (e.g. UMTS), users in the cell will have some quality of service requirements. Hence, if the user with the best channel condition is always scheduled, scheduling will be very unfair from the user point of view. A simple scheduling algorithm called *proportional fair scheduling* is developed to cope with this fairness problem while trying to exploit the multiuser diversity at the same time.

This scheduler does not use current SINR as a scheduling metric directly but aims to normalize the SINR value by dividing it with the past average throughput for that user. Hence, even if a user has a higher mean SINR all the time he is not going to be scheduled dominantly.

Let the past average throughput of a user i at time k be $P_i(k)$, then the proportional fair scheduler (PFS) will choose the user j according to following formula:

$$j = arg \max_i \left(\frac{\gamma_i(k)}{P_i(k)} \right) \tag{2.4}$$

The average throughput term $P_i(k)$ can be obtained by using a recursive average with forgetting factor $1/T_c$.

$$P_i(k+1) = \begin{cases} (1 - 1/T_c) \cdot P_i(k) + 1/T_c \cdot R_i(k) & j = i \\ (1 - 1/T_c) \cdot P_i(k) & j \neq i \end{cases} \tag{2.5}$$

This scheduler can be seen as a modified version of the *maximum SINR scheduler*. As already mentioned, in this scheduling algorithm users do not compete for resources according to their requested rates but normalized requested rates according to their past average throughputs are used. As can be seen in figure 2.2 this scheduler automatically schedules a user when the user channel quality is near its own peaks. This phenomenon is also important for opportunistic beam forming which is discussed in the next section.

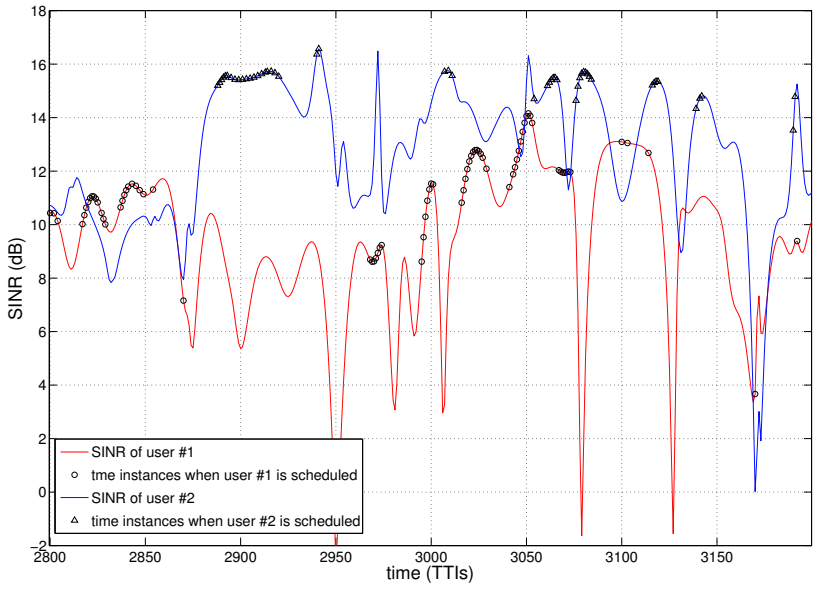

Figure 2.2: Scheduling instances of 2 users in a cell with 5 users.

Another important parameter in 2.5 is T_c time constant. T_c defines the time window that the averaging is made upon. A large time window means a better representation of the past throughput. But, from the other side value of T_c is directly proportional to the length of time that a user may not be scheduled. That is, if T_c is chosen too large a user may not receive data for long time that he cannot afford from the QoS point of view. And if T_c is choosen too small, scheduler will converge to *Round-Robin scheduler* and hence multiuser diversity may not be exploited, especially if variance of mean values of user SINR values are high. At this point an example from HSDPA can be given [6]. The HSDPA bearer capacity gain for proportional fair scheduling over simple round robiun in time scheduling is of the order of 40-60% for macro cell environments, and can be theoretically higher for certain environments and operating conditions [7]. Figure 2.3 presents the relative performance between Release '99 and HSDPA in two different environments.

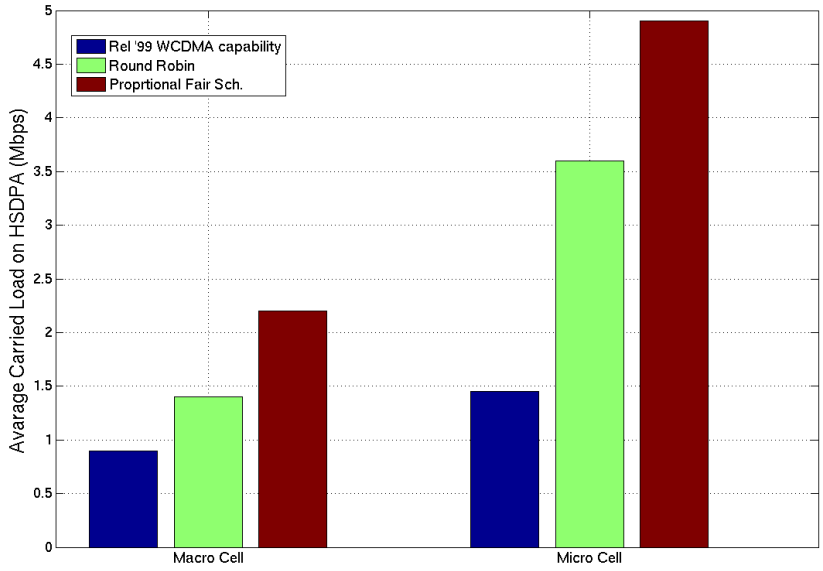

Figure 2.3: HSDPA and Release '99 performance comparison

2.2 Mobility , Feedback Delay and Estimation Filters

2.2.1 Mobility and Feedback Delay

In chapters 2.1.1 and 2.1.2 it was shown that users are scheduled when their channel quality is at its local peak with respect to time constant T_c. Keeping $\mathbb{E}\left[|h|^2\right]$ constant, figure 2.4 shows that the amount of multiuser diversity gain is different for different mobility environments.

This is intuitive because if $\mathbb{E}\left[|h|^2\right]$ is constant higher speed means more channel dynamics and hence higher peaks. And, driving those higher peaks higher system throughput can be obtained. But this does not mean that the higher the mobility of the users the more throughput we have. Again in figure 2.4 it can be seen that when the users move at a speed of 30km/h, system throughput gets worse. This is because the receiver has trouble tracking and predicting the channel variations, so that the predicted channel is a low-pass smoothed version of the actual fading process [5].

There are two major reasons for that. First, for the receiver as the fluctuations become more and more intensive it becomes very difficult to estimate the channel variations and the feedback sent to the transmitter in order to make proportional fair scheduler work becomes actually a rough estimate of

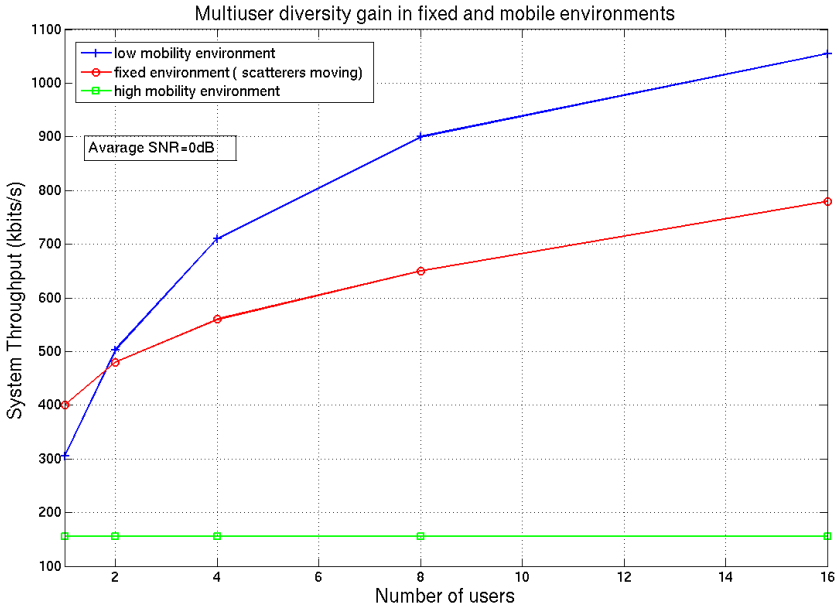

Figure 2.4: Effect of mobility on multiuser diversity gain

the actual channel condition. Moreover, the delay time that is required for this feedback information to be measured and sent to transmitter becomes very effective on the performance. In figure 2.5, it is shown how increasing channel dynamics also increases the feedback information error.

Note also that, SINR is used as a measurement of channel quality, while in real systems this may be a little bit different. e.g. HSDPA uses channel quality indicator (CQI) as a feedback information but relations and challenges remain unchanged since these are very close to each other.

2.2.2 Discrete-time Causal Wiener Filter

Wiener Filter is the linear, time-invariant filter that minimizes $\mathbb{E}\left[\varepsilon^2\right]$, the variance of the error. According to figure 2.6 the output of the filter can be written as:

$$y_k = \sum_{l=0}^{M-1} (w_l x_{k-l}) \tag{2.6}$$

then from the minimized error equation it follows

$$\begin{aligned}
\mathbb{E}\left[\varepsilon^2\right] &= \mathbb{E}\left[(d_k - y_k)^2\right] = \mathbb{E}\left[\left(d_k - \sum_{l=0}^{M-1}(w_l x_{k-l})\right)^2\right] \\
&= \mathbb{E}\left[d_k^2\right] - 2\sum_{l=0}^{M-1}(w_l \mathbb{E}\left[d_k x_k\right]) + \sum_{l=0}^{M-1}\left(\sum_{l=0}^{M-1}(w_l w_m \mathbb{E}\left[x_{k-l} xk - m\right])\right) \\
\mathbb{E}\left[\varepsilon^2\right] &= r_{dd}(0) - 2\sum_{l=0}^{M-1}(w_l r_{dx}(l)) + \sum_{l=0}^{M-1}\left(\sum_{m=0}^{M-1}(w_l w_m r_{xx}(l-m))\right)
\end{aligned} \tag{2.7}$$

where

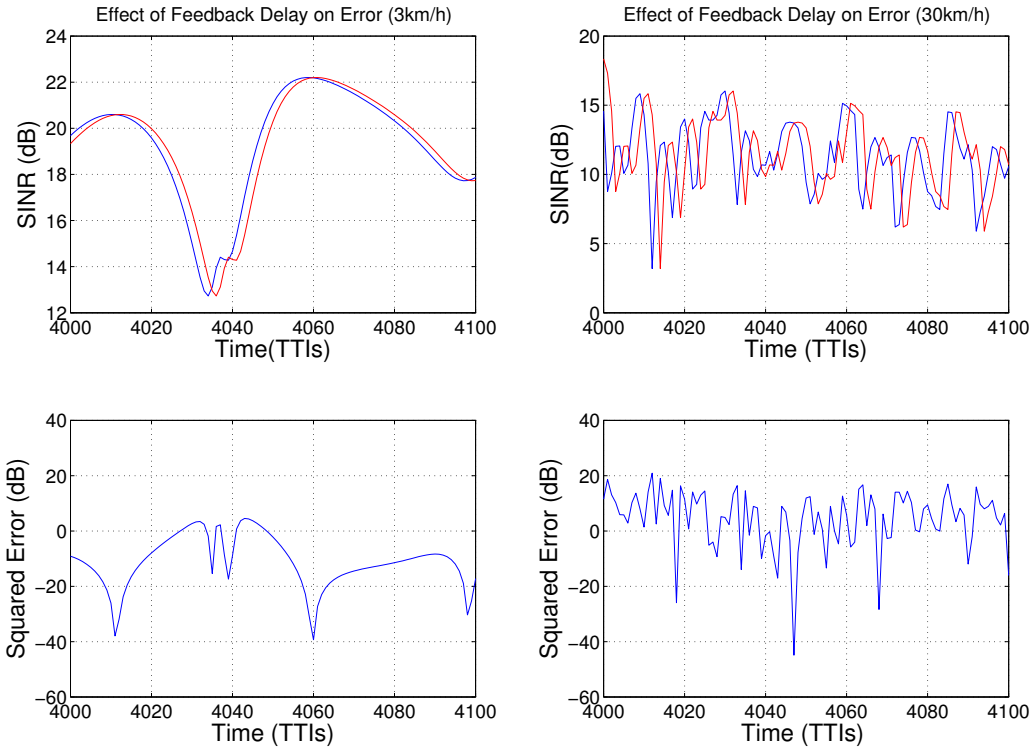

Figure 2.5: Effect of feedback delay for users at 3km/h and 30km/h

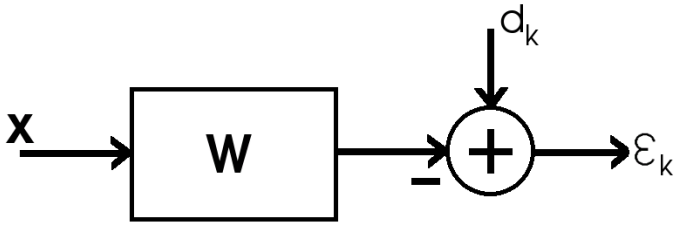

Figure 2.6: Wiener Filter

$$\begin{aligned} r_{dd}(0) &= \mathbb{E}\left[d_k^2\right] \\ r_{dx}(l) &= \mathbb{E}\left[d_k x_{k-l}\right] \\ r_{xx}(l-m) &= \mathbb{E}\left[x_k x_{k+l-m}\right] \end{aligned} \tag{2.8}$$

equation 2.7 can be written in matrix form as

$$\mathbb{E}\left[\varepsilon^2\right] = r_{dd}(0) - 2\boldsymbol{P}\boldsymbol{W}^T + \boldsymbol{W}^T R \boldsymbol{W} \tag{2.9}$$

where

$$\boldsymbol{P} = \begin{bmatrix} r_{dx}(0) \\ r_{dx}(1) \\ \vdots \\ r_{dx}(M-1) \end{bmatrix} \tag{2.10}$$

$$\boldsymbol{R} = \begin{bmatrix} r_{xx}(0) & r_{xx}(1) & \dots & \dots & r_{xx}(M-1) \\ r_{xx}(1) & r_{xx}(0) & \ddots & \ddots & \vdots \\ \vdots & \ddots & \ddots & \ddots & \vdots \\ \vdots & \ddots & \ddots & r_{xx}(0) & r_{xx}(1) \\ r_{xx}(M-1) & \dots & \dots & r_{xx}(1) & r_{xx}(0) \end{bmatrix} \tag{2.11}$$

to derive the optimum filter $\boldsymbol{W_{opt}}$ e the gradient of the error with respect to the weight vector $\boldsymbol{w}$ is calculated and equated to zero.

$$\nabla\left(\varepsilon^2\right) = \begin{bmatrix} \dfrac{\partial}{\partial w_0}\left(\varepsilon^2\right) \\ \dfrac{\partial}{\partial w_1}\left(\varepsilon^2\right) \\ \vdots \\ \dfrac{\partial}{\partial w_{M-1}}\left(\varepsilon^2\right) \end{bmatrix} \tag{2.12}$$

and setting $\nabla = -2\boldsymbol{P} + 2R\boldsymbol{W}$ equal to zero we have

$$\boldsymbol{W_{opt}}R = \boldsymbol{P} \Rightarrow \boldsymbol{W_{opt}} = R^{-1}\boldsymbol{P} \tag{2.13}$$

Note that one usually does not know $\boldsymbol{R}$ and $\boldsymbol{P}$. Therefore, in most practical applications they are estimated and our application is not an exception. In the simulator that was used for this thesis, an RLS estimator whose origin is coming from the Wiener-Filter is implemented in order to keep convergence time of the adaptive filter and hence simulation time short. The purpose of utilizing such an adaptive filter is to compansate the effect of feedback delay that was discussed in chapter 2.2.1.

2.2.3 RLS Filter

In chapter 2.2.2 the theory behind the Wiener Filter was discussed. In simulator that gives results in chapter 4, an RLS (Recursive Least Squares) estimator was used which is coming from this filter approach. This choice was made because of its relative short convergence time. Below a detailed derivation of the RLS algorithm is given to make the meaning of parameters that will be discussed in following results clear.

Define a cost function to be minimised as

$$\mathcal{E}(n) = \sum_{i=1}^{n} \lambda^{n-i}|e(i)|^2 \tag{2.14}$$

where λ is the forgetting factor. It is in general used to ensure that data in the distant past are forgotten in order to afford the possibility of following the statistical variations of the observable data when the filter operates in a nonstationary environment.It has the property that

$$0 < \lambda^{n-i} \leq 1, \qquad i = 1, 2, \dots, n \tag{2.15}$$

and note that $\lambda = 1$ means infinte memory. n is the variable length of the observable data and $e(i)$ is defined by

$$\begin{aligned} e(i) &= d(i) - y(i) \\ &= d(i) - \mathbf{w}^H(n)\mathbf{u}(i) \end{aligned} \tag{2.16}$$

where

$$\mathbf{u}(i) = [u(i), u(i-1), \ldots, u(i-M+1)]^T \tag{2.17}$$

is the tap input vector and

$$\mathbf{w}(n) = [w_0(n), w_1(n), \ldots, w_{M-1}(n)]^T \tag{2.18}$$

is the tap weight vectoe at time n.

The optimum value of the tap weight vector $\mathbf{w}(n)$, for which the cost function $\mathcal{E}(n)$ attains its minimum value is defined by the normal equations written in matrix form as

$$\mathbf{\Phi}(n)\mathbf{w}(n) = \mathbf{z}(n) \tag{2.19}$$

Here $\mathbf{\Phi}(n)$ is the $M \times M$ correlation matrix defined as

$$\mathbf{\Phi}(n) = \sum_{i=1}^{n} \lambda^{n-i}\mathbf{u}(i)\mathbf{u}^H(i) \tag{2.20}$$

and $\mathbf{z}(n)$ is the $M \times 1$ cross-correlation vector defined as

$$\mathbf{z}(n) = \sum_{i=1}^{n} \lambda^{n-i}\mathbf{u}(i)d^*(i) \tag{2.21}$$

To compute the least-square estimate of the $\mathbf{w}(n)$ from the equation 2.19, inverse of the correlation matrix $\mathbf{\Phi}(n)$ has to be determined. Hovever this inversion can be computationally very complex and hence time consuming. In order to avoid this *Woodbury's identity* can be used.

This identity states that for the two positive definite $M \times M$ matrices related by

$$\mathbf{A} = \mathbf{B}^{-1} + \mathbf{C}\mathbf{D}^{-1}\mathbf{C}^H \tag{2.22}$$

where $\mathbf{D}$ is another positive definite $N \times M$ matrix, $\mathbf{A}^{-1}$ can be written as follows

$$\mathbf{A}^{-1} = \mathbf{B} - \mathbf{B}\mathbf{C}(\mathbf{D} + \mathbf{C}^H\mathbf{B}\mathbf{C})^{-1}\mathbf{C}^H\mathbf{B} \tag{2.23}$$

This identity can be used easily if we write $\mathbf{\Phi}(n)$ as

$$\mathbf{\Phi}(n) = \lambda\mathbf{\Phi}(n-1) + \mathbf{u}(n)\mathbf{u}^H(n) \tag{2.24}$$

and take

$$\begin{aligned} \mathbf{A} &= \mathbf{\Phi}(n) \\ \mathbf{B} &= \lambda\mathbf{\Phi}(n-1) \\ \mathbf{C} &= \mathbf{u}(n) \\ \mathbf{D} &= 1 \end{aligned} \tag{2.25}$$

Then inverse of $\mathbf{\Phi}(n)$ can be written as

$$\mathbf{P}(n) = \lambda^{-1}\mathbf{P}(n-1) - \lambda^{-1}\mathbf{k}(n)\mathbf{u}^H(n)\mathbf{P}(n-1) \tag{2.26}$$

where $\mathbf{P}(n) = \mathbf{\Phi}^{-1}(n)$ and

$$\mathbf{k}(n) = \frac{\lambda^{-1}\mathbf{P}(n-1)\mathbf{u}(n)}{1 + \lambda^{-1}\mathbf{u}^H(n)\mathbf{P}(n-1)\mathbf{u}(n)} \tag{2.27}$$

Now that inverse of $\mathbf{\Phi}(n)$ is computed, from equation 2.19 we can derive a recursive formula for $\mathbf{w}(n)$ as follows.

First rewrite equation 2.21 as

$$\mathbf{z}(n) = \lambda\mathbf{z}(n-1) + \mathbf{u}(n)d^*(n) \tag{2.28}$$

then

$$\begin{aligned}
\mathbf{w}(n) &= \mathbf{\Phi}^{-1}(n)\mathbf{z}(n) \\
&= \mathbf{P}(n)\mathbf{z}(n) \\
&= \lambda\mathbf{P}(n)\mathbf{z}(n-1) + \mathbf{P}(n)\mathbf{u}(n)d^*(n) \\
&= \mathbf{P}(n-1)\mathbf{z}(n-1) - \mathbf{k}(n)\mathbf{u}^H(n)\mathbf{P}(n-1)\mathbf{z}(n-1) + \mathbf{P}(n)\mathbf{u}(n)d^*(n) \\
&= \mathbf{\Phi}^{-1}(n-1)\mathbf{z}(n-1) - \mathbf{k}(n)\mathbf{u}^H(n)\mathbf{\Phi}^{-1}(n-1)\mathbf{z}(n-1) + \mathbf{P}(n)\mathbf{u}(n)d^*(n) \\
&= \mathbf{w}(n-1) - \mathbf{k}(n)\mathbf{u}^H(n)\mathbf{w}(n-1) + \mathbf{P}(n)\mathbf{u}(n)d^*(n) \\
&= \mathbf{w}(n-1) + \mathbf{k}(n)\left[d^*(n) - \mathbf{u}^H(n)\mathbf{w}(n-1)\right] \\
&= \mathbf{w}(n-1) + \mathbf{k}(n)\xi^*(n)
\end{aligned} \tag{2.29}$$

where $\xi(n)$ is the a priori estimation error defined by

$$\begin{aligned}
\xi(n) &= d(n) - \mathbf{u}^T(n)\mathbf{w}^*(n-1) \\
&= d(n) - \mathbf{w}^H(n-1)\mathbf{u}(n)
\end{aligned} \tag{2.30}$$

Signal flow graph of the algorithm is given in figure 2.7 and a summary is given in table 2.1. In figure 2.8 performance of a sample SINR estimation is given for a feedback delay of 3 TTIs.

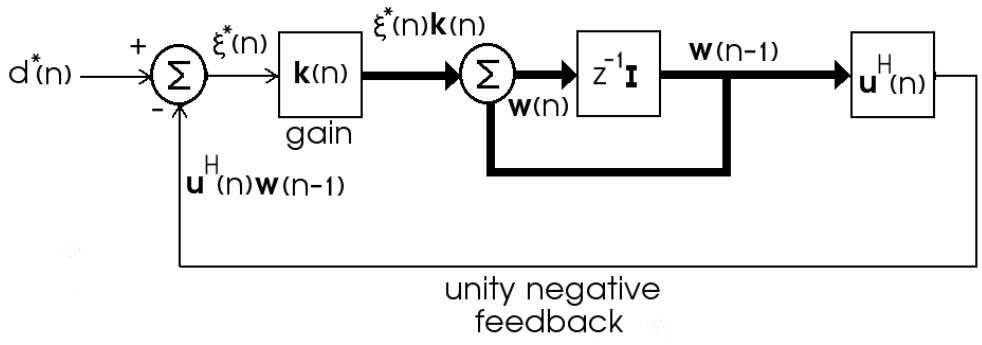

Figure 2.7: Signal flow graph of the RLS algorithm

Summary of the RLS Algorithm

Initialize the algorithm by setting

$\mathbf{P}(0) = \delta^{-1}\mathbf{I}$, δ is a small positive constant

$\mathbf{w}(0) = \mathbf{0}$

For each instant of time $n = 1, 2, \ldots$ compute

$$\mathbf{k}(n) = \frac{\lambda^{-1}\mathbf{P}(n-1)\mathbf{u}(n)}{1 + \lambda^{-1}\mathbf{u}^H(n)\mathbf{P}(n-1)\mathbf{u}(n)}$$

$\xi(n) = d(n) - \mathbf{w}^H(n-1)\mathbf{u}(n)$

$\mathbf{w}(n) = \mathbf{w}(n-1) + \mathbf{k}(n)\xi^*(n)$

$\mathbf{P}(n) = \lambda^{-1}\mathbf{P}(n-1) - \lambda^{-1}\mathbf{k}(n)\mathbf{u}^H(n)\mathbf{P}(n-1)$

Table 2.1: RLS Algorithm

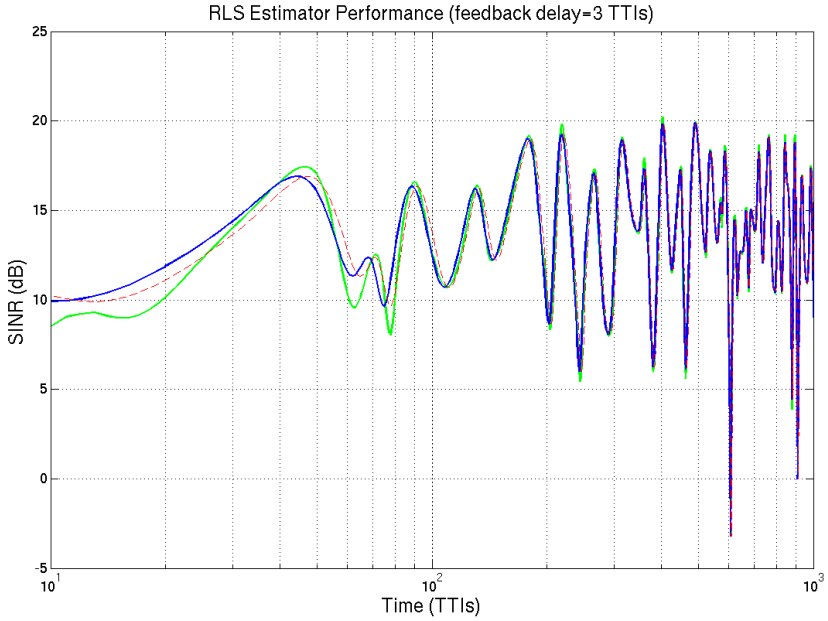

Figure 2.8: SINR estimation sample for feedback delay of 3 TTIs

2.3 Opportunistic Beamforming

In chapter 2.2.1 it was discussed that together with the PFS scheduler, increased channel dynamics can increase the system throughput. So in case of low channel dynamics idea of increasing channel dynamics artificially comes into mind. A general mathematical explanation of this idea is given in [1] as follows.

Consider a system with n_t transmit antennas at the base station and let $h_{lk}[m]$ be the complex channel gain from antenna l to the user k in time m. At this time m signal $x[m]$ is transmitted from all antennas but it is first multiplied by a complex number $\sqrt{\alpha_l[m]}e^{j\theta_l[m]}$ at antenna l, for $l = 1, \ldots, n_t$ such that $\sum_{l=1}^{n_t} \alpha_l[m] = 1$, in order to keep transmit power fixed. Then the received signal at the user k can be written as

$$y_k[m] = \left(\sum_{l=1}^{n_t} \sqrt{\alpha_l[m]}e^{j\theta_l[m]}h_{lk}[m]\right) x_m[m] + w_k[m] \tag{2.31}$$

Vector consisting of $\sqrt{\alpha_l\,[m]}e^{j\theta_l[m]}$ elements for $l = 1, \ldots, n_t$ wil be called as the weight vector, since it determines how power is distributed among the elements of antenna array.

$$\boldsymbol{w}\,[m] := \begin{bmatrix} \sqrt{\alpha_1\,[m]}e^{j\theta_1[m]} \\ \vdots \\ \sqrt{\alpha_{n_t}\,[m]}e^{j\theta_{n_t}[m]} \end{bmatrix} \tag{2.32}$$

Rate of change of $\alpha_1\,[m]$ and $\theta_1\,[m]$ with respect to time is very important for the performance of opportunistic beamforming. Although increased channel dynamics may increase the total system throughput, in chapter 2.2.1 it was also discussed that it will make the effect of feedback delay more severe. Three points that should be taken care of while designing $\boldsymbol{w}$ are [1]

1. $\boldsymbol{w}\,[m]$ should change as fast as possible to provide full channel fluctuation within the latency time of interest.
2.The variation should be slow enough and should happen at a time scale that allows the channel to be reliably estimated by the users and the SNR feed-back.

There are different approaches possible in choice of $\alpha_1\,[m]$ and $\theta_1\,[m]$ variation. Three of them will be discussed, namely *isotropic beamforming*, *phase-shift beamforming* and *phased array beamforming* among which isotropic beam forming and phase-shift beamforming will be more important as the system emerges into MIMO.

Isotropic beamforming: In isotropic BF case $\boldsymbol{w}$ simply consists of normalized i.i.d. complex Gaussian entries which can be written as

$$\boldsymbol{w_{iso}}\,[m] = \frac{\boldsymbol{w_n}\,[m]}{\sqrt{\boldsymbol{w_n^H}\,[m] \cdot \boldsymbol{w_n}\,[m]}} \tag{2.33}$$

where $\boldsymbol{w_n}\,[m] \sim \mathcal{CN}(0, 1)$.

Note that since elements of $\boldsymbol{w}$ are i.i.d complex Gaussian entries, it is possible for an antenna to have 0 power or all the power available at any particular time. This variation of power for one antenna makes the hardware design of such a system difficult.

Phase-shift beamforming: For the phase-shift beamforming case taking care of even distribution of power among T antennas a weight vector can be defined as follows

$$\boldsymbol{w_{phs}}\,[m] = \frac{1}{\sqrt{T}}\begin{pmatrix} 1 & e^{j\theta[m]} \ldots e^{j(T-1)\theta[m]} \end{pmatrix}^T \tag{2.34}$$

This approach will be particularly useful in MIMO extension, hence is worth keeping in mind.

Phased array beamforming: In the case of fully correlated channels neither isotropic beamforming nor phase-shift beamforming is optimal. In such cases phased array beamforming is proposed and is given by

$$\boldsymbol{w_{pharr}}\,[m] = \frac{1}{\sqrt{T}}\begin{pmatrix} 1 & e^{j2\pi d \sin\varphi[m]} & \ldots & e^{j2\pi d(T-1)\sin\varphi[m]} \end{pmatrix}^T \tag{2.35}$$

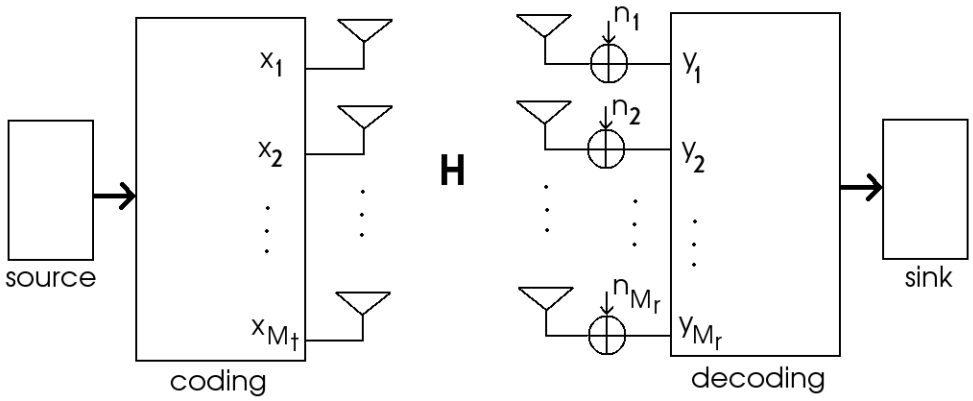

Figure 2.9: Block diagram of a $M_t \times M_r$ MIMO system

2.4 Extension of OBF to MIMO Systems

Figure 2.9 shows the block diagram of a $M_t \times M_r$ wireless MIMO system. Here the received signal vector $\boldsymbol{y}$ can be written in terms of the transmitted signal vector $\boldsymbol{x}$ as

$$\boldsymbol{y} = \boldsymbol{H}\boldsymbol{x} + \boldsymbol{n} \tag{2.36}$$

where $\boldsymbol{H}$ is a $M_t \times M_r$ complex channel matrix and $\boldsymbol{n}$ is the AWGN vector with covariance $N_0\boldsymbol{I}_{\boldsymbol{M_r}}$.Under suitable fading conditions having multiple antennas both at the transmitter and receiver side (MIMO) yields an additional spatial dimension and hence provides a degree of freedom gain [8]. In fact, in [5] the capacity of a MIMO channel is given by

$$C = \sum_{i=1}^{n_{min}} \log\left(1 + \frac{P_i^* \lambda_i^2}{N_o}\right) \text{ bits/s/Hz} \tag{2.37}$$

where λ_i are the singular values of the MIMO channel matrix $\boldsymbol{H}$, $n_{min} = min\left(M_t, M_r\right)$, P_i^* are the power allocation coefficients where $\sum_i P_i^* = P$. Similarity of this equation to equation 2.1 for MISO systems is worth considering. Derivation of the above equation via singular value decomposition is given in the folllowing chapter. It leads to some very interesting and useful facts that will become handy also in opportunistic beamforming.

2.4.1 Capacity of a MIMO System via singular value decomposition

Consider equation 2.36. Assuming $\mathbf{H}$ is a linear transformation, linear algebra tells us that every linear transformation can be represented as a composition of a rotation, a scaling and another rotation operation [5]. Those three operations can be obtained by *singular value decomposition* of that matrix which can be written as follows:

$$\mathbf{H} = \mathbf{U}\mathbf{\Lambda}\mathbf{V}^* \tag{2.38}$$

where $\mathbf{U} \in \mathbb{C}^{M_t \times M_r}$ and $\mathbf{V} \in \mathbb{C}^{M_t \times M_r}$ are unitry matrices and $\mathbf{\Lambda} \in \mathbb{R}^{M_t \times M_r}$ is a rectangular matrix whose diagonal elements are non-negative real numbers and whose off-diagonal elements are zero. Diagonal elements $\lambda_1 \geq \lambda_2 \ldots \geq \lambda_{n_{min}}$ are called as the ordered *singular values* of matrix $\mathbf{H}$. Since also

$$\mathbf{H}\mathbf{H}^* = \mathbf{U}\mathbf{\Lambda}\mathbf{\Lambda}^t\mathbf{U}^* \tag{2.39}$$

holds, which means that squared singular values are the eigenvalues of the matrix $\mathbf{HH}^*$. Now if we define

$$\mathbf{x}' := \mathbf{V}^*\mathbf{x} \tag{2.40}$$

$$\mathbf{y}' := \mathbf{U}^*\mathbf{y} \tag{2.41}$$

$$\mathbf{n}' := \mathbf{U}^*\mathbf{n} \tag{2.42}$$

then we can write equation 2.36 as

$$\mathbf{y}' = \mathbf{\Lambda}\mathbf{x}' + \mathbf{n}' \tag{2.43}$$

Considering above equation it can be shown that [5] $\mathbf{n}' \sim \mathcal{CN}(0, N_o\mathbf{I}_{\mathbf{n_r}})$ has the same distribution as $\mathbf{n}$. and $\|\mathbf{x}'\|^2 = \|\mathbf{x}\|^2$. Thus energy is preserved after this coordinate transformation and we have an equivalent representation of the MIMO channel in terms of parallel channels which can mathematically be represented with the following equation

$$y_i' = \lambda_i x_i' + n_i', \qquad i = 1, 2, \ldots n_{min} \tag{2.44}$$

where n_{min} is the number of singular values. Figure 2.10 gives a block diagram of the equivalent system according to the derivations above.

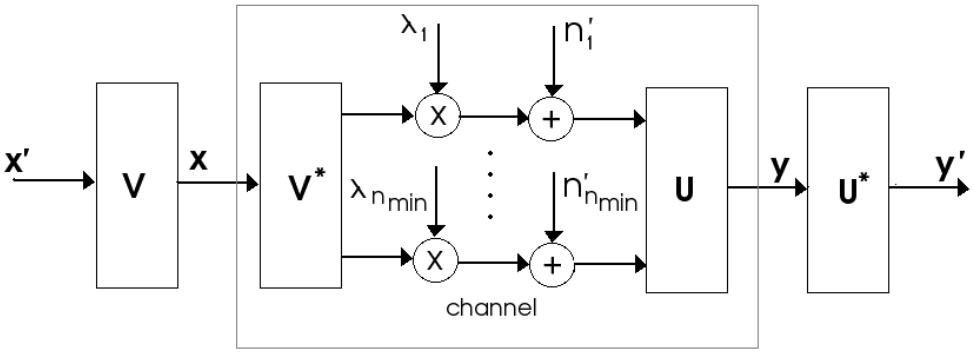

Figure 2.10: Converting a MIMO channel into a parallel channel through SVD

2.4.2 MIMO signal model with OBF

In subsection 2.3 $\boldsymbol{w}$, the weight vector is discussed. Note that in a MIMO system input $\boldsymbol{x}$ is a vector since it can have more than one stream and also note that there is a $M_t \times M_r$ complex channel matrix $\boldsymbol{H}$. Therefore, in MIMO systems in order to apply a similar opportunistic beamforming idea like in MISO systems a *beamforming matrix* $\boldsymbol{W}$ has to be used.

Hence, block diagram of the transmitter side of a MIMO system with opportunistic beamformig looks like figure 2.11.

So, received signal vector $\boldsymbol{y}$ becomes

$$\boldsymbol{y} = \boldsymbol{HWx} + \boldsymbol{n} \tag{2.45}$$

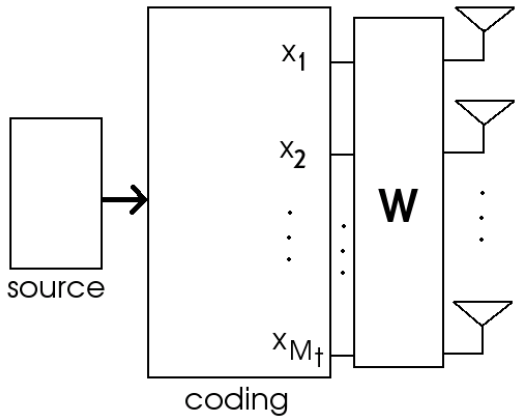

Figure 2.11: Block diagram of the transmitter side of a $M_t \times M_r$ MIMO system

Due to the limited total power at the transmitter there is a constraint on the norm of the $\boldsymbol{W}$. Assuming total power is P this can be derived as follows

$$\begin{aligned} P \geq \mathbb{E}\left\{ \mid \boldsymbol{W}\boldsymbol{x} \mid^2 \right\} &= \mathbb{E}\left\{ \boldsymbol{x}^H \boldsymbol{W}^H \boldsymbol{W}\boldsymbol{x} \right\} \\ &= \mathbb{E}\left\{ tr\left(\boldsymbol{W}\boldsymbol{x}\boldsymbol{x}^H \boldsymbol{W}^H \right) \right\} \\ &= tr\left(\mathbb{E}\left\{ \boldsymbol{W}\boldsymbol{x}\boldsymbol{x}^H \boldsymbol{W}^H \right\} \right) \\ &= tr\left(\boldsymbol{W}\mathbb{E}\left\{ \boldsymbol{x}\boldsymbol{x}^H \right\} \boldsymbol{W}^H \right) \end{aligned}$$

if we replace $\mathbb{E}\left\{ \boldsymbol{x}\boldsymbol{x}^H \right\}$ with σ_x^2 we have

$$P \geq tr\left(\boldsymbol{W}\boldsymbol{W}^H \right) \cdot \sigma_x^2 = \|\boldsymbol{W}\|_F^2 \cdot \sigma_x^2 \tag{2.46}$$

where $\| \circ \|_F^2$ denotes the *Frobenius norm*.

If there is more than one data stream and assuming power is identically distributed among those streams in signal vector $\boldsymbol{x}$, $\sigma_x^2 = P/M_t$ can be written and equation 2.46 becomes

$$\|\boldsymbol{W}\|_F^2 \leq M_t \tag{2.47}$$

2.4.3 MIMO Channel Modeling

In order to create spatially and temporally correlated waveform to represent the channel, first a very long waveform consisting of Rayleigh distributed channel coefficients is created. Temporal correlation of these waveforms are dependent on the user speed. Then a randomly selected slice of this waveform is used as the fading between each transmitter and receiver antenna combination. Hence, at this level fading between any antenna combination is temporally correlated but not spatially correlated yet.

Then spatial correlation of these fading waveforms are achieved by multiplying these processes by the square-root of the spatial correlation matrix which has Laplacian or uniform power angular density (PAD) depending on the scenerio choice.

For a theoretical explanation of this, first consider a system with M_t antennas at one side and a single antenna at the other side. For the sake of simplicity, further assume that the side with uniform linear array of antennas (ULA) is the BS side and the side with a single antenna is mobile side, hence a MISO system. While extending this to MIMO system, this constraint will be dropped.

Local Scattering Model: In a cellular system like for example UMTS where a BS transmits to several MSs in a cell, BS does not see the MS from a discrete azimuthal direction but under a normal mean direction and a certain angular spread [9] [10] [11] [12]. This is due to scatterers around the MS and if any also due to scaterrers around BS. The most commonly used way of modelling such a phonemon is the so-called *local scattering model*. [13] A visualization of such an environment with a normal mean direction θ and a certain angular spread ζ is given in figure 2.12.

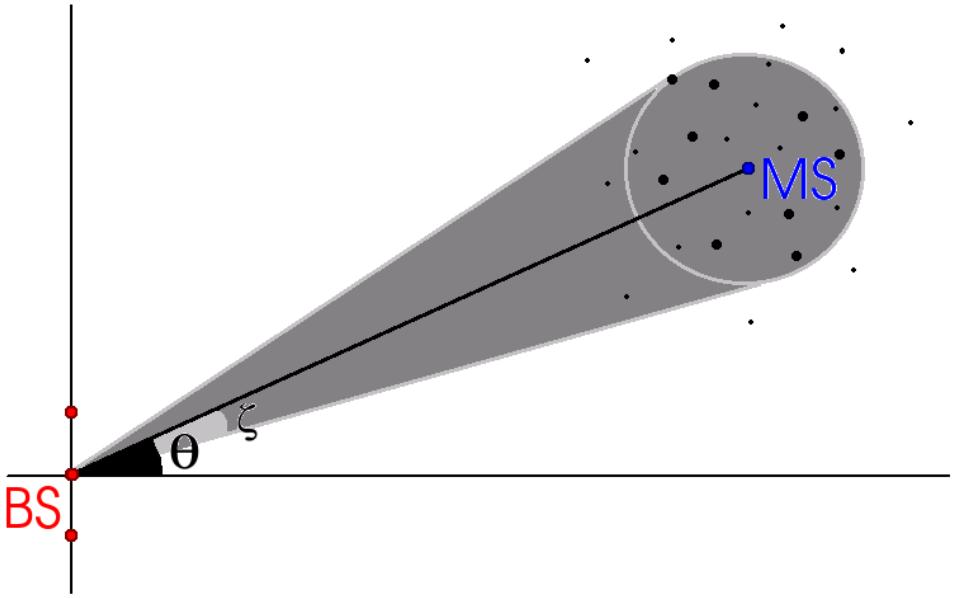

Figure 2.12: Physical scattering model with generic scatterer distribution. Transmitted signal exhibits a angular spread ζ around the mean angle of departure (mean azimuth) θ .

Channel Covariance Matrix: At the beginning of chapter 2.4.3 it was mentioned that first a temporally correlated but spatially uncorrelated channel is created and than spatial correlation with channel covariance matrix $\boldsymbol{R}$ is applied. Mathematical proof of that can be given as follows:

First the received signal is writen in a frequency non-selective signal model at time instant m at the receiver k as

$$r_m^{(k)} = \boldsymbol{w}_l^{(k)} \boldsymbol{h}_m^{(k)} a_m + n_m^{(k)} \tag{2.48}$$

where $\boldsymbol{w}_l \in \mathbb{C}^{M_t \times 1}$ is the weight vector and $\boldsymbol{h_m^{(k)}} = \left[h_{1:m}^{(k)} \dots h_{M_t:m}^{(k)}\right] \in \mathbb{C}^{M_t \times 1}$ is the physical channel vector between the BS and user k, a_m is the transmitted symbol and $n_m^{(k)}$ is AWGN. From the above equation with dropping k for the sake of convenience, it can be shown that the expected received SNR conditioned on a bemforming vector $\boldsymbol{w}$ is given by [14].

$$\begin{aligned} \gamma(\boldsymbol{w}) &= \mathbb{E}\left[\boldsymbol{w}^H \boldsymbol{h}\boldsymbol{h}^H \boldsymbol{w} | \boldsymbol{w}\right] \\ &= \boldsymbol{w}^H \boldsymbol{R} \boldsymbol{w} \end{aligned} \tag{2.49}$$

$\boldsymbol{R} = \mathbb{E}\left[\boldsymbol{h}\boldsymbol{h}^H\right]$ can be created as follows. First consider $\boldsymbol{h'_m} = \left[h'_{1:m} \dots h'_{M_t:m}\right] \in \mathbb{C}^{M_t \times 1}$ vector consists of spatially uncorrelated entries. Then define $\boldsymbol{R}_{sp}^{1/2}$ matrix whose entries are the envelope correlation between two respective antenna elements.

$$R_{i,j} := \rho\,(i-j) = \mathbb{E}\left[h_i h_j^*\right] \tag{2.50}$$

then from

$$\begin{aligned}\boldsymbol{R} &= \mathbb{E}\left[\boldsymbol{h}\boldsymbol{h}^H\right] \\ &= \mathbb{E}\left[\boldsymbol{R}_{sp}^{1/2}\boldsymbol{h}'\boldsymbol{h}'^H\boldsymbol{R}_{sp}^{1/2H}\right] \\ &= \boldsymbol{R}_{sp}^{1/2}\mathbb{E}\left[\boldsymbol{h}'\boldsymbol{h}'^H\right]\boldsymbol{R}_{sp}^{1/2H} \\ &= \boldsymbol{R}_{sp}\end{aligned} \tag{2.51}$$

follows and spatial correlation matrix can be obtained.

In general if antennas i and j are d' units apart then the envelope correlation of these two can be shown to be [15] [16] [17] [12].

$$\rho(d) = \int_{-\pi}^{\pi} e^{-j2\pi d\sin(\theta)} p(\theta) d\theta \tag{2.52}$$

where θ is the azimuth angle of the transmitted or the received signal component with respect to the array braodside direction, $p(\theta)$ is its probability density funnction and $d = d'/\lambda$ is the normalised antenna seperation. $p(\theta)$ is determined by the distribution of the scaterrers that are mentioned in *local scattering model* and figure 2.12. There are several $p(\theta)$ distributions that lead to different envelope correlations considered here, namely *uniform ring distribution, uniform azimuth distribution, uniform disc distribution, Gaussian spatial distribution, Laplacian distribution.*

2.4.3.1 Uniform ring distribution

This model assumes a ring of uniformly distributed scatterers at a fixed distance R from the mobile terminal. [13] [15]. $p(\theta)$ of this scatterer distribution is given by [16]

$$p(\theta) = \begin{cases} \dfrac{1}{\pi\sqrt{\zeta^2 - (\theta-\phi_0)^2}} & -\zeta + \phi_0 < \theta < \zeta + \phi_0 \\ 0, & otherwise \end{cases} \tag{2.53}$$

2.4.3.2 Uniform azimuth distribution

This distribution was proposed by Clarke and Jakes [18] [15]. It assumes uniform azimuth distribution within an angular spread $\pm\zeta$ around the azimuth angle ϕ_0. The pad of this scatterer distribution is given as follows:

$$p(\theta) = \begin{cases} \dfrac{1}{2\zeta} & -\zeta + \phi_0 < \theta < \zeta + \phi_0 \\ 0, & otherwise \end{cases} \tag{2.54}$$

2.4.3.3 Uniform disc distribution

This scatterer distribution function assumes a uniform spatial pdf of the scatterers in a disc with radius R around the mobile [19] [20]. Associated $p(\theta)$ is given as follows:

$$p(\theta) = \begin{cases} \dfrac{2\cos(\theta-\phi_0)\sqrt{\sin^2(\zeta)-\sin^2(\theta-\phi_0)}}{\pi\sin^2(\zeta)} & -\zeta+\phi_0 < \theta < \zeta+\phi_0 \\ 0, & otherwise \end{cases} \tag{2.55}$$

2.4.3.4 Gaussian spatial distribution

Up to now all the scattering models discussed assumed somehow a symmetry, but it is argued that relevant scatterers are more likely to be close to MS, hence Gaussian spatial distribution is proposed. [21] [22] [23] [24] $p(\theta)$ of this kind of distribution which is an approximation to exact solution is called truncated Gaussian pdf and is given as follows [1]:

$$p(\theta) = \begin{cases} \dfrac{Q_G}{\sqrt{2\pi\sigma^2}} exp\left(-\dfrac{(\theta-\phi_0)^2}{2\sigma^2}\right), & -\pi/2+\phi_0 \le \theta \le \pi/2+\phi_0 \\ 0, & otherwise \end{cases} \tag{2.56}$$

where Q_G is a normalisation constant for a probability density function.

2.4.3.5 Laplacian spatial distribution

At this one scatterers are assumed to have Laplacian spatial distribution. This is the scaterrer distribution that is most commonly used in our simulator. This type of distribution is also proposed in 3GPP TR 25.996 v 6.1.0 [25].

$$p(\theta) = \begin{cases} k \cdot exp\left(-\dfrac{\sqrt{2}\mid\theta-\phi_0\mid}{\zeta}\right), & -\pi/2+\phi_0 \le \theta \le \pi/2+\phi_0 \\ 0, & otherwise \end{cases} \tag{2.57}$$

[1] interested reader can find the exact pdf at Appendix A.4

From the beginning of chapter 2.4.3 up to this point a MISO system is considered. Above discussions can also be extended to MIMO. In order to do this first consider the equation 2.36. Take $\boldsymbol{H}$ in this equation as.

$$\boldsymbol{H} = \begin{bmatrix} \alpha_{11} & \alpha_{12} & \dots & \dots & \alpha_{1M_r} \\ \alpha_{21} & \alpha_{22} & \ddots & \ddots & \vdots \\ \vdots & \ddots & \ddots & \ddots & \vdots \\ \vdots & \ddots & \ddots & \alpha_{(M_t-1)(M_r-1)} & \alpha_{(M_t-1)M_r} \\ \dots & \dots & \dots & \alpha_{(M_t)(M_r-1)} & \alpha_{M_tM_r} \end{bmatrix} \tag{2.58}$$

Here α_{mn} is the complex transmission coefficient from antenna m at the MS to antenna n at the BS. Then, if it is assumed that all the antenna elements in two arrays of this MIMO system have the same polarization and same radiation pattern, the spatial complex correlation coefficient at the BS between antenna m_1 and m_2 is given by [26]

$$\rho^{BS}_{m_1m_2} = \langle \alpha_{m_1n}, \alpha_{m_1n} \rangle \tag{2.59}$$

where $\langle a, b \rangle$ computes the correlation coefficient between a and b. Similarly the spatial complex correlation coeficient observed at the MS is given by

$$\rho^{MS}_{n_1n_2} = \langle \alpha_{mn_1}, \alpha_{mn_2} \rangle \tag{2.60}$$

Note that 2.59 is assumed to be independent of n and 2.60 is assumed to be independent of m. Now keeping the above 2 equations in mind, following symmetrical complex correlation matrices can be written for either side.

$$\boldsymbol{R}_{BS} = \begin{bmatrix} \rho^{BS}_{11} & \rho^{BS}_{12} & \dots & \rho^{BS}_{1M_t} \\ \rho^{BS}_{21} & \rho^{BS}_{22} & \dots & \rho^{BS}_{2M_t} \\ \vdots & \vdots & \ddots & \vdots \\ \rho^{BS}_{M_t1} & \rho^{BS}_{M_t2} & \dots & \rho^{BS}_{M_tM_t} \end{bmatrix} \tag{2.61}$$

$$\boldsymbol{R}_{MS} = \begin{bmatrix} \rho^{MS}_{11} & \rho^{MS}_{12} & \dots & \rho^{MS}_{1M_r} \\ \rho^{MS}_{21} & \rho^{MS}_{22} & \dots & \rho^{MS}_{2M_r} \\ \vdots & \vdots & \ddots & \vdots \\ \rho^{MS}_{M_t1} & \rho^{MS}_{M_t2} & \dots & \rho^{MS}_{M_tM_t} \end{bmatrix} \tag{2.62}$$

And now similar to 2.59 and 2.60 the correlation coefficient between two arbitrary transmission coefficients connecting two different sets of antennas is given as [26]

$$\rho^{n_1m_1}_{n_2m_2} = \langle \alpha_{m_1n_1}, \alpha_{m_2n_2} \rangle \tag{2.63}$$

In [26], it is shown that the above equation can be modelled as

$$\rho^{n_1m_1}_{n_2m_2} = \rho^{MS}_{n_1n_2} \rho^{BS}_{m_1m_2} \tag{2.64}$$

which means that *the spatial correlation matrix of the MIMO radio channel is the Kronecker product of the spatial correlation matrix at the MS ans BS* and brings the following very important formula for our MIMO channel model.

$$\boldsymbol{R}_{MIMO} = \boldsymbol{R}_{MS} \otimes \boldsymbol{R}_{BS} \tag{2.65}$$

Application of this $\boldsymbol{R}_{MIMO}$ to the system in order ro create spatial correlation is follows.

Consider $\mathbf{a}_{MN\times 1} = [a_1, a_2, \cdots, a_{MN}]^T$ where a_{mn} are zero mean complex , independent and identically distributed RVs. Which can be considered as the spatially uncorrelated MIMO channel coefficients in vector form. Then define $\mathbf{A}_{MN\times 1} = [\alpha_{11}, \alpha_{21}, \cdots, \alpha_{M1}, \alpha_{12}, \cdots, \alpha_{MN}]^T$ whose elements are nothing but the elements of $\boldsymbol{H}$ matrix. Having defined the relation between $\mathbf{A}$ and $\boldsymbol{H}$, $\mathbf{A}$ is created according to

$$\mathbf{A} = \mathbf{Ca} \tag{2.66}$$

where

$$\boldsymbol{R}_{MIMO} = \mathbf{C}\mathbf{C}^T \tag{2.67}$$

That is, $\mathbf{C}$ can be created by Cholesky factorization of $\boldsymbol{R}_{MIMO}$ provided that $\boldsymbol{R}_{MIMO}$ is nonsingular.

2.4.4 Receiver Processing

In this chapter the derivations of SINR in case of several different MIMO receiver algorithms for a $M_t \times M_r$ MIMO system are given.

2.4.4.1 Maximum Ratio Combining (MRC)

In MRC only one data stream can be send, so signal model at the sender is given as follows:

$$\boldsymbol{x}(t) = \sqrt{\varepsilon P_t}\boldsymbol{w}s(t) \tag{2.68}$$

where $\mathbb{E}^2\{s(t)\} = 1$, $\boldsymbol{w}^H\boldsymbol{w} = 1$ and $\sqrt{\varepsilon P_t}$ term represents the part of the total power allocated to the data signal $s(t)$.

at the receiver side following signal is received:

$$\boldsymbol{r}_u(t) = \sum_{i=1}^{N} \boldsymbol{H}_{u,i}\boldsymbol{x}(t-\tau_i) + \boldsymbol{i}_{IC}(t) + \boldsymbol{n}(t) \tag{2.69}$$

where

$$\boldsymbol{H}_{u,i} = \begin{bmatrix} h_{11}^{u,i} & h_{12}^{u,i} & \dots & h_{1M_r}^{u,i} \\ h_{21}^{u,i} & h_{22}^{u,i} & \dots & h_{2M_r}^{u,i} \\ \vdots & \vdots & \ddots & \vdots \\ h_{M_t1}^{u,i} & h_{M_t2}^{u,i} & \dots & h_{M_tM_t}^{u,i} \end{bmatrix} \tag{2.70}$$

Substituting equation 2.68 into equation 2.69 we have

$$\begin{aligned}\boldsymbol{r}_u(t) &= \sum_{i=1}^{N} \boldsymbol{H}_{u,i}\sqrt{\varepsilon P_t}\boldsymbol{w}s(t-\tau_i) + \boldsymbol{i}_{IC}(t) + \boldsymbol{n}(t) \\ &= \sum_{i=1}^{N} \boldsymbol{h}_{u,i}^{eff} s(t-\tau_i) + \boldsymbol{i}_{IC}(t) + \boldsymbol{n}(t) \\ &= h_{u,1}^{eff} s(t) + \sum_{i=2}^{N} \boldsymbol{h}_{u,i}^{eff} s(t-\tau_i) + \boldsymbol{i}_{IC}(t) + \boldsymbol{n}(t) \end{aligned} \tag{2.71}$$

where the second term after $h_{u,i}^{eff}s(t)$ is the multipath term and will be written as $\boldsymbol{i}_{MP}(t)$ hereafter. $\boldsymbol{r}_u(t)$ is the vector of the signals that are received at the antennas of the receiver side. These signals must be processed to obtain $s(t)$ as good as possible. Call the vector that is applied to the received signal vector as $\boldsymbol{r}$. Then we have

$$d_u(t) = \boldsymbol{r}^H \boldsymbol{r}_u(t) \tag{2.72}$$

when we substitute $\boldsymbol{r}_u(t)$ that can be rewritten as

$$d_u(t) = \boldsymbol{r}^{\boldsymbol{H}} \boldsymbol{h}_{u,1}^{eff} s(t) + \boldsymbol{r}^H \boldsymbol{i}_{MP}(t) + \boldsymbol{r}^H \boldsymbol{i}_{IC}(t) + \boldsymbol{r}^H \boldsymbol{n}(t) \tag{2.73}$$

and from here we write SINR as

$$SINR = \frac{\mathbb{E}\left\{\boldsymbol{r}^H \boldsymbol{h}_{u,1}^{eff} s(t) s^*(t) \boldsymbol{h}_{u,1}^{effH} \boldsymbol{r}\right\}}{\boldsymbol{r}^H \left(\mathbb{E}\left\{\boldsymbol{i}_{MP}(t)\boldsymbol{i}_{MP}^H(t)\right\} + \mathbb{E}\left\{\boldsymbol{i}_{IC}(t)\boldsymbol{i}_{IC}^H(t)\right\} + \mathbb{E}\left\{\boldsymbol{n}(t)\boldsymbol{n}^H(t)\right\}\right)\boldsymbol{r}} \tag{2.74}$$

For the sake of simplicity this equation can be written in matrix form as

$$SINR = \frac{\boldsymbol{r}^H \boldsymbol{S} \boldsymbol{r}}{\boldsymbol{r}^H \left(\boldsymbol{I}_{MP} + \boldsymbol{I}_{IC} + \boldsymbol{N}\right)\boldsymbol{r}} \tag{2.75}$$

Note that, here SINR is maximized if $\boldsymbol{r} = \boldsymbol{h}_{u,1}^{eff}$ which is nothing but MRC.

2.4.4.2 ZF and MMSE Receivers

In case of *zero forcing* and *minimum mean square* receivers SINR derivation is similar but in this case there are more than one stream. So $s(t)$ becomes $\boldsymbol{s}(t)$ and $\boldsymbol{w}$ vector becomes $\boldsymbol{W}$ matrix. Then transmitted signal follows

$$\boldsymbol{x}(t) = \sqrt{\varepsilon P_t}\boldsymbol{W}\boldsymbol{s}(t) \tag{2.76}$$

where $tr\left\{\boldsymbol{W}\boldsymbol{W}^H\right\} = 1$, and $\mathbb{E}\left\{\boldsymbol{s}(t)\boldsymbol{s}^H(t)\right\} = \boldsymbol{I}$. From here the received signal $\boldsymbol{r}_u(t)$ at the receiver can be written and SINR derivation is done very similar to previous chapter.

$$\begin{aligned}\boldsymbol{r}_u(t) &= \sum_{i=1}^{N} \boldsymbol{H}_{u,i} x(t-\tau_i) + \boldsymbol{i}_{IC}(t) + \boldsymbol{n}(t) \\ &= \sum_{i=1}^{N} \boldsymbol{H}_{u,i} \sqrt{\varepsilon P_t} \boldsymbol{W} s(t-\tau_i) + \boldsymbol{i}_{IC}(t) + \boldsymbol{n}(t) \\ &= \sum_{i=1}^{N} \boldsymbol{H}_{u,i}^{eff} s(t-\tau_i) + \boldsymbol{i}_{IC}(t) + \boldsymbol{n}(t) \\ &= \boldsymbol{H}_{u,1}^{eff} s(t) + \sum_{i=2}^{N} \boldsymbol{H}_{u,i}^{eff} s(t-\tau_i) + \boldsymbol{i}_{IC}(t) + \boldsymbol{n}(t) \end{aligned} \tag{2.77}$$

Again calling second term in the above equation $\boldsymbol{i}_{MP}(t)$ which represents multipath interference we can proceed to receiver processing algorithm. This time receiver processing matrix applied at the receiver to the received signal vector is called as $\boldsymbol{R}$ and we have

$$\boldsymbol{d}_u(t) = \boldsymbol{R}\boldsymbol{r}_u(t) \tag{2.78}$$

where $\boldsymbol{d}_u(t) = [d_1(t) \quad d_2(t) \ldots d_s(t) \ldots d_i(t)]^T$, i being the number of data streams sent. Substituting 2.77 below equation follows

$$d_s(t) = \left[\boldsymbol{R}\boldsymbol{H}_{u,1}^{eff} \boldsymbol{s}(t)\right]_s + \left[\boldsymbol{R}\left(\boldsymbol{i}_{MP}(t) + \boldsymbol{i}_{IC}(t) + \boldsymbol{n}(t)\right)\right]_s \tag{2.79}$$

where $[\circ]_s$ operator takes the s^{th} row of the matrix it is applied to.

Remember at the beginning of this section it was mentioned that in case of ZF and MMSE more than one data stream can be sent. This is an important gain but comes with an expense of additional interference. Namely, *interstream interference*. For the mathematical reason of that, consider the first term of the equation 2.79. Noise and interference terms are not carried here for the sake of simplicity.

$$d_s(t) = \left[\boldsymbol{R}\boldsymbol{H}_{u,1}^{eff} \boldsymbol{s}(t)\right]_s + \ldots = \left[\boldsymbol{A}\boldsymbol{s}(t)\right]_s + \ldots \tag{2.80}$$

where

$$\boldsymbol{A} = \begin{bmatrix} a_{11} & a_{12} & \ldots & a_{1N} \\ a_{21} & a_{22} & \ldots & a_{2N} \\ \vdots & \vdots & \ddots & \vdots \\ a_{N1} & a_{N2} & \ldots & a_{NN} \end{bmatrix} \tag{2.81}$$

and N is the number of data streams sent. In this case $d_s(t)$ can be written as follows

$$d_s(t) = a_{ss} s_s(t) + \sum_{j=1, j\neq s}^{N} a_{sj} s_j(t) + \ldots \tag{2.82}$$

and second term is the interstream interference that was mentioned. This $\mathbb{I}_{IS}(t)$ is written with a different font to indicate that it is not the interference that is received by any antenna before processing but an interference after receiver processing. That is, after $\boldsymbol{R}$ is applied. Then the SINR term for the s^{th} stream can be written as follows

$$SINR_s = \frac{\mathbb{E}\left\{a_{ss}s_s(t)s_s^H(t)a_{ss}^H(t)\right\}}{\mathbb{E}\left\{\mathbb{I}_{IS}(t)\mathbb{I}_{IS}^H(t)\right\} + \mathbb{E}\left\{\left[\mathbf{R}\left(\boldsymbol{i}_{MP}(t)+\boldsymbol{i}_{IC}(t)+\boldsymbol{n}(t)\right)\left(\boldsymbol{i}_{MP}(t)+\boldsymbol{i}_{IC}(t)+\boldsymbol{n}(t)\right)^H\mathbf{R}^H\right]_{ss}\right\}} \tag{2.83}$$

and $[\circ]_s$ s operator takes the s^{th} component of the diagonal of the matrix that it is applied to. Above equation can be written in matrix form as

$$SINR_s = \frac{\mathbb{E}\left\{a_{ss}s_s(t)s_s^H(t)a_{ss}^H(t)\right\}}{\mathbb{E}\left\{\mathbb{I}_{IS}(t)\mathbb{I}_{IS}^H(t)\right\} + \left[\mathbf{R}\left(\boldsymbol{I}_{MP}+\boldsymbol{I}_{IC}+\boldsymbol{N}\right)\mathbf{R}^H\right]_{ss}} \tag{2.84}$$

The difference between ZF and MMSE receiver is the choice of $\mathbf{R}$ matrix. While ZF receiver simply tries to apply the inverse of the channel matrix, MMSE behaves like a matched filter under low SNR conditions and like a ZF receiver under high SNR conditions. [2].

ZF receiver: Assuming $\boldsymbol{H}_{u,1}^{eff}$ is invertible the matrix $\mathbf{R}$ for the zero forcing case is

$$\mathbf{R} = \left(\boldsymbol{H}_{u,1}^{eff}\right)^{-1} \tag{2.85}$$

and if $\boldsymbol{H}_{u,1}^{eff}$ is not invertible, pseudoinverse of $\boldsymbol{H}_{u,1}^{eff}$ can be taken as $\mathbf{R}$.

MMSE receiver: MMSE receiver tries to take care of both noise term and signal term. So $\mathbf{R}$, that minimizes the MSE can be written as combination of 2 matrices as

$$\mathbf{R}_{opt}^H = \mathbf{C}_{rr}^{-1} \cdot \mathbf{C}_{sr} \tag{2.86}$$

where

$$\mathbf{C}_{rr} = \mathbb{E}\left\{\mathbf{r}_u\mathbf{r}_u^H\right\} = \boldsymbol{S} + \boldsymbol{I}_{MP} + \boldsymbol{I}_{IC} + \boldsymbol{N} \tag{2.87}$$

and

$$\mathbf{C}_{sr} = \mathbb{E}\left\{\mathbf{r}_u\mathbf{s}^H\right\} = \mathbb{E}\left\{\left(\boldsymbol{H}_{u,1}^{eff} + \boldsymbol{i}_{MP}(t) + \boldsymbol{i}_{IC}(t) + \boldsymbol{n}(t)\right)\mathbf{s}^H(t)\right\} \tag{2.88}$$

which is nothing but $\boldsymbol{H}_{u,1}^{eff}$. So $\mathbf{R}_{opt}^H$ can be written as

$$\mathbf{R}_{opt}^H = \left(\boldsymbol{S} + \boldsymbol{I}_{MP} + \boldsymbol{I}_{IC} + \boldsymbol{N}\right)^{-1} \cdot \boldsymbol{H}_{u,1}^{eff} \tag{2.89}$$

2.4.5 Opportunistic Beamforming Matrix in MIMO

In chapters 2.3 and 2.4 some opportunistic beamforming approaches for MISO and capacity of a MIMO system via singular value decomposition were discussed. Using the information of those chapters, in this chapter two different approaches to create the so called weight matrix ($\mathbf{W}$) for opportunistic beamforming will be discussd.

[2] A very detailed anyalysis and comparison of these two receive algorithms can be found in [5]

2.4.6 MIMO Phase Shift Beamforming Approach

The idea behind this approach is exactly the same as in 2.34. Basically seperate weight vectors are written for each stream or each antenna. In 2×2 case MIMO opportunistic beam-forming matrix is given as follows. Note that, since magnitude of each entry of the matrix is always 1, 2.47 is automatically satisfied.

$$\boldsymbol{W}_2[m] = \frac{1}{\sqrt{2}} \begin{bmatrix} 1 & 1 \\ e^{j\theta[m]} & -e^{j\theta[m]} \end{bmatrix} \tag{2.90}$$

where $\frac{1}{\sqrt{2}}$ is the normalisation factor and is equak to $\frac{1}{\sqrt{n}}$ in general for $\boldsymbol{W}_n$.

Here as can be seen $\theta[m]$ is changing at each TTI and $\theta[m] = \theta[m-1] + \Delta\theta$, $\Delta\theta$ is taken as design parameter. It defines how fast opportunistic beamforming will be. Figure 2.13 shows the effect of changing $\Delta\theta$ on SINR fluctuation rate.

Equation 2.90 can be extended for higher number of antennas using the Kronecker product. Remember that this matrix product is defines as

$$\boldsymbol{A} \otimes \boldsymbol{B} = \begin{bmatrix} a_{11}\boldsymbol{B} & a_{12}\boldsymbol{B} & \dots & a_{1n}\boldsymbol{B} \\ a_{21}\boldsymbol{B} & a_{22}\boldsymbol{B} & \dots & a_{2n}\boldsymbol{B} \\ \vdots & \vdots & \ddots & \vdots \\ a_{m1}\boldsymbol{B} & a_{m2}\boldsymbol{B} & \dots & a_{mn}\boldsymbol{B} \end{bmatrix} \tag{2.91}$$

Given $\boldsymbol{W}_2$ matrix in 2.90 and the Kronecker product we can find any matrix $\boldsymbol{W}_{2n}$ as

$$\boldsymbol{W}_{2n} = \boldsymbol{W}_2 \otimes \boldsymbol{W}_n \tag{2.92}$$

where n is even.

Here it can be easily proven that $\boldsymbol{W}_{2n}$ matrix is unitary $\forall n, n \epsilon \mathbb{Z}^+$.

First for $n = 1$

$$\begin{aligned} \boldsymbol{W}_2 \cdot \boldsymbol{W}_2^H = & \\ & \frac{1}{\sqrt{2}} \begin{bmatrix} 1 & 1 \\ e^{j\theta[m]} & -e^{j\theta[m]} \end{bmatrix} \cdot \frac{1}{\sqrt{2}} \begin{bmatrix} 1 & e^{-j\theta[m]} \\ 1 & -e^{-j\theta[m]} \end{bmatrix} \\ & = \frac{1}{2} \begin{bmatrix} 2 & 0 \\ 0 & 2 \end{bmatrix} \\ & = \mathbf{I} \end{aligned} \tag{2.93}$$

now assuming that

$$\boldsymbol{W}_n \cdot \boldsymbol{W}_n^H = \mathbf{I} \tag{2.94}$$

consider

$$
\begin{aligned}
\boldsymbol{W}_{2n} \cdot \boldsymbol{W}_{2n}^{H} = & \\
& \frac{1}{\sqrt{2n}} \begin{bmatrix} \boldsymbol{W}_n & \boldsymbol{W}_n \\ \boldsymbol{W}_n e^{j\theta[m]} & -\boldsymbol{W}_n e^{j\theta[m]} \end{bmatrix} \cdot \frac{1}{\sqrt{2}} \begin{bmatrix} \boldsymbol{W}_n^H & \boldsymbol{W}_n^H e^{-j\theta[m]} \\ \boldsymbol{W}_n^H & -\boldsymbol{W}_n^H e^{-j\theta[m]} \end{bmatrix} \\
& = \frac{1}{2n} \begin{bmatrix} 2n\mathbf{I} & \bigcirc \\ \bigcirc & 2n\mathbf{I} \end{bmatrix} \\
& = \mathbf{I}
\end{aligned} \tag{2.95}
$$

where $\bigcirc$ represents a zero matrix. Hence, it is proven that $\boldsymbol{W}_{2n}$ is a unitary matrix in general. As an example $\boldsymbol{W}_4$ is given in the following equation.

$$
\boldsymbol{W}_4[m] = \frac{1}{2} \begin{bmatrix} 1 & 1 & 1 & 1 \\ e^{j\theta[m]} & -e^{j\theta[m]} & e^{j\theta[m]} & -e^{j\theta[m]} \\ e^{j\theta[m]} & e^{j\theta[m]} & -e^{j\theta[m]} & -e^{j\theta[m]} \\ e^{j2\theta[m]} & -e^{j2\theta[m]} & -e^{j2\theta[m]} & e^{j2\theta[m]} \end{bmatrix} \tag{2.96}
$$

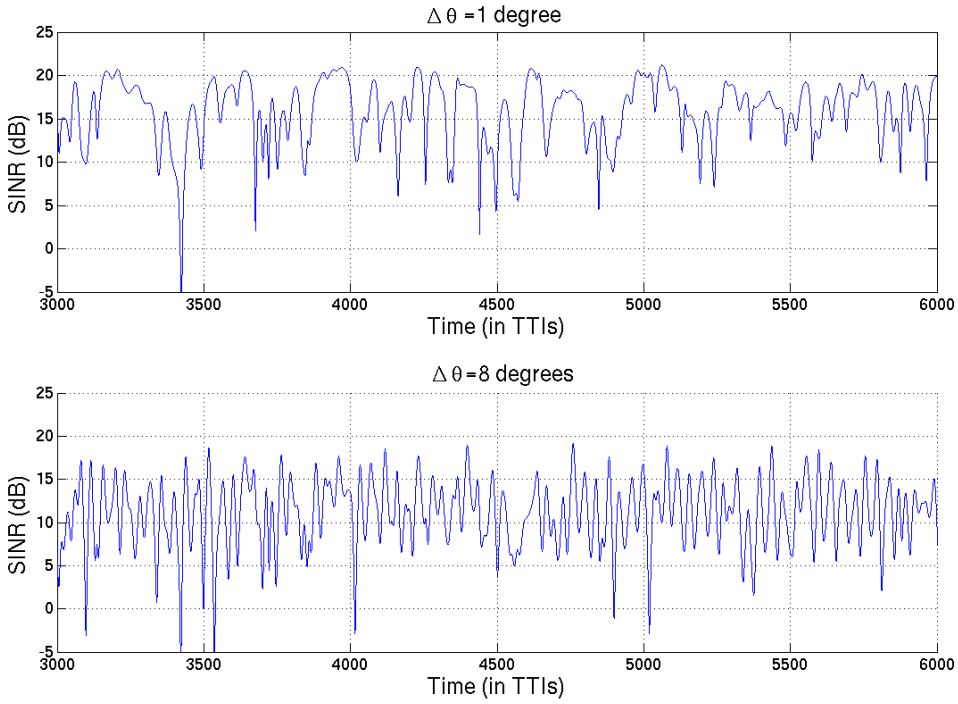

Figure 2.13: SINR of a user under the same slow and fast fading conditions for 2 different W matrices at different speeds.

2.4.7 Channel SVD Beamforming Approach

Remember equation 2.38 in which it was shown that a MIMO channel matrix can be written in terms of three operations. Namely, rotation, scaling and rotation. Here the second matrix $\mathbf{V}^*$ is a unitary matrix and multiplication of a unitray matrix with another unitary matrix is again a unitary matrix. [3]

[3] Because $U \cdot U^* = I$ and hence $U_1 U_2 U_2^* U_1^* = U_1 U_1^* = I$

So if the signal vector $\mathbf{x}$ is multiplied with a somehow randomly changing unitary matrix V_U following derivation holds

$$\begin{aligned} \boldsymbol{y} &= \boldsymbol{HW}\boldsymbol{x} + \boldsymbol{n} \\ &= \boldsymbol{HV}_U^*\boldsymbol{x} + \boldsymbol{n} \\ &= \mathbf{U}\boldsymbol{\Lambda}\mathbf{V}^*\boldsymbol{V}_U^*\boldsymbol{x} + \boldsymbol{n} \\ &= \mathbf{U}\boldsymbol{\Lambda}\boldsymbol{V}_{OBF}^*\boldsymbol{x} + \boldsymbol{n} \\ &= \boldsymbol{H}_{OBF}\boldsymbol{x} + \boldsymbol{n} \end{aligned} \tag{2.97}$$

The purpose of this simple substitution is to show that with a proper $\mathbf{W}$ matrix an effective MIMO channel with different and preferably increased channel dynamics can be created. Rate of change of the unitary matrix is a design parameter. As we previously discussed in MISO case, it should not be slower than current channel dynamics but also cannot be too fast. Hence, in the simulator it is created according to this:

First a fast fading channel for a virtual user is created. Then depending on the speed wanted, this waveform which assures temporal correlation that is very important for scheduler and estimator in case of feedback delay is resampled. After that, computing singular value decomposition of the channel matrix gives temporally correlated unitary matrices which are nothing but the $\mathbf{V}_U$ matrices in derivation 2.97.

Channel SVD beamforming approach is a more randomised idea that takes a virtual user (or may be more) as a reference and aims for increasing channel dynamics. This and similar opportunistic beamforming ideas arising from SVD of the MIMO channel are discussed in [2], [3]. *Equivalent speed* term in this thesis is used meaning that $\boldsymbol{W}$ is created from a virtual user at that speed. Since $\boldsymbol{W}$ is a result of SVD and applied on the existing channel, it cannot be said that channel directly becomes as if users are moving at that speed. Hence, it should be kept in mind that equivalent speed is a loosely used term and will be picked up at chapter . In figure 2.14 change of SINR fluctuation rate under two different speeds is given.

2.5 UMTS/HSDPA Fundamentals

2.5.1 WCDMA in Third Generation Systems

First generation systems were mostly analog cellular systems. Second generation systems are digital systems and are still in use. GSM, PDC, cdmaOne (IS-95) and US-TDMA (IS-136) can be given as examples of 2nd generation systems. Third generation systems are designed for multimedia communication. Services associated with third generation systems provide the ability to transfer simultaneously both voice data (a telephone call) and non-voice data (such as downloading information, exchanging email, and instant messaging). In marketing 3G services, video telephony has often been used as the killer application for 3G [6].

2.5.1.1 WCDMA Radio Channels

The channel organisation the WCDMA uses is a three layer one. There are *logical channels*, *transport channels* and *physical channels*. Logical channels describe the type of information to be transmitted, transport channels describe how the information on the logical channels are to be transferred and the physical channels are the transmission media providing the radio platform.

Figure xxx gives the logical, transport and the physical channel mapping in WCDMA. The mandatory transport channels are Broadcast channel (BCH), Pagong Channel (PCH), Forward Access Channel

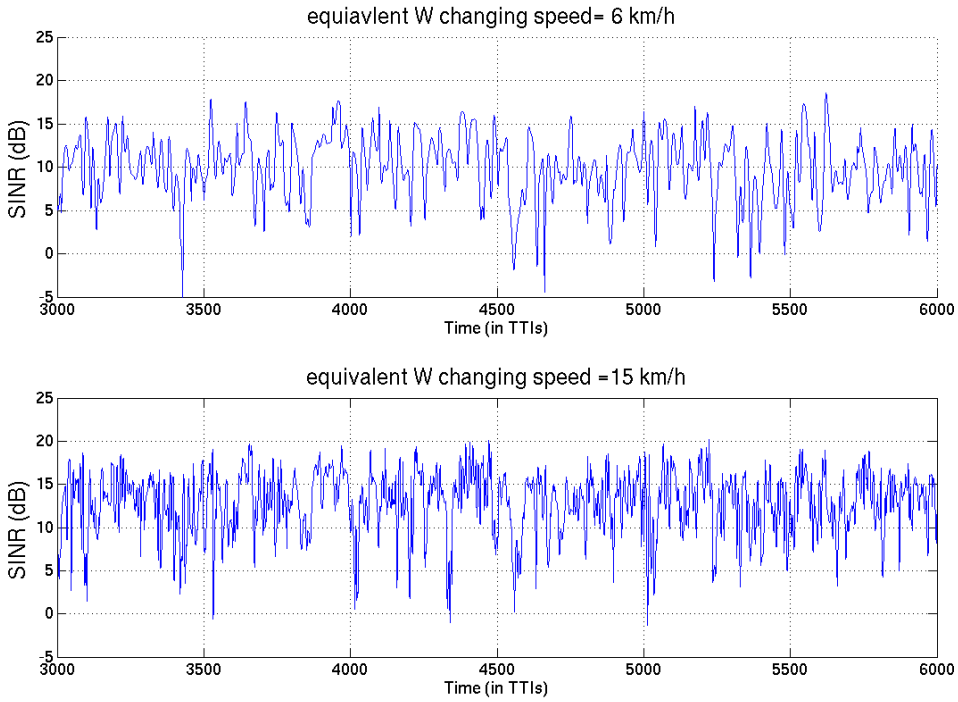

Figure 2.14: SINR of a user moving at 3km/h under the same slow and fast fading conditions for 2 different W matrices at different equivalent speeds.

(FACH) and Dedicated Channel (DCH). In addition to these, the operator may configure UTRA to use the Downlink Shared Channel (DSCH) [4].

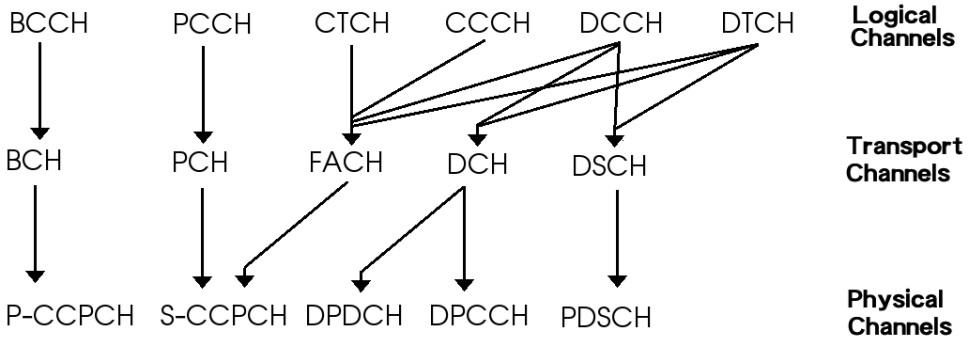

Figure 2.15: Logical, transport and physical channel mapping in the downlink direction.

In the uplink direction there are only three logical channels., CCCH, DTCH and DCCH. Figure 2.16.

2.5.2 UMTS Radio Access Network (UTRAN)

Figure 2.17 illustrates the UTRAN architecture on the network element level. UTRAN consists of Radio Network Subsystems (RNS) and each RNS contains various amount of Base Stations (Node B) realising the Uu interface and one Radio Network Controller (RNC).

[4]The shared HSDPA data channel (HS-PDSCH) is a more capable upgrade of the Release 99 - specified Downlink Shared Channel (DSCH)

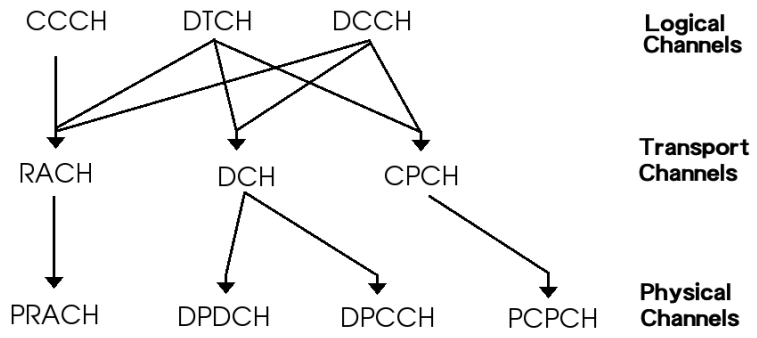

Figure 2.16: Logical, transport and physical channel mapping in the uplink direction.

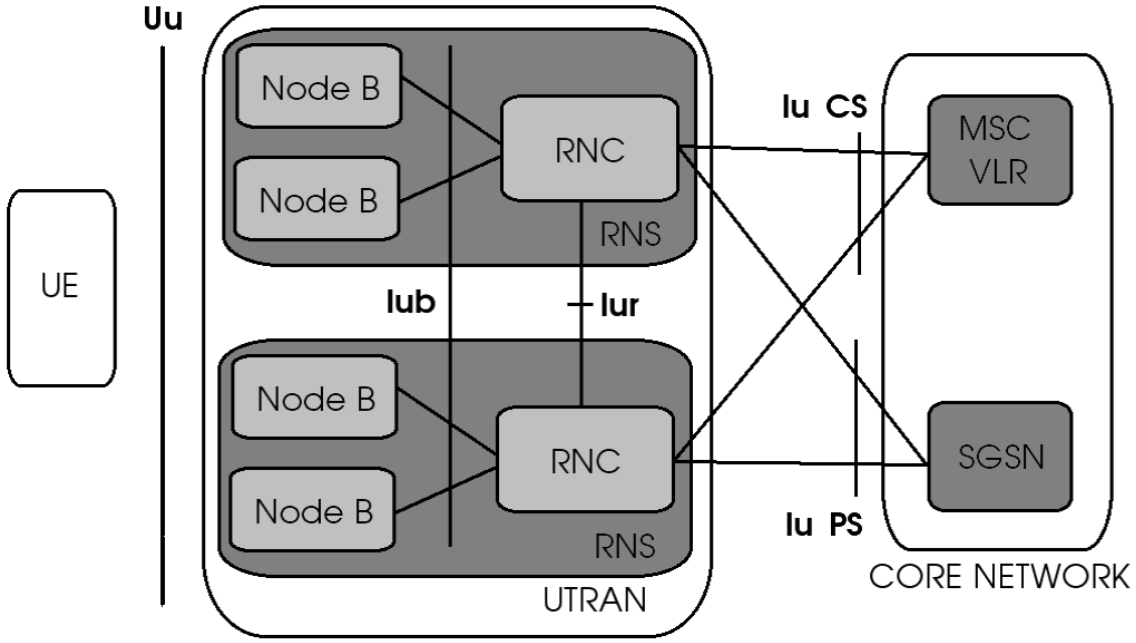

Figure 2.17: UTRAN Architure

Node B

Main tasks of a Node B are to establish the physical implementation of the Uu interface and, towards the network, the implementation of the Iub interface by utilising the protocol stacks specified for these interfaces. [27]

Radio Network Controller

The RNC is the network element responsible for the control of the radio resources of UTRAN. It interfaces the core network and also terminates the radio resource control protocol that defines the massages and procedures between the mobile and UTRAN.

2.5.3 HSDPA

A typical user of a 3G system is more likely to use the downlink of the system more than the uplink [5]. (web brosing, games etc.) and a 3G system can accomodate only a few maximum data rate users at a time before the capacity runs out in the downlink direction. HSDPA aims to improve downlink capacity, and thus finds a solution to this requirement. HSDPA increases both the the system capacity as a whole and the data rate that can be allocated for one user. In addition to increased capacity, HSDPA also provides shorter delays. User perception of a fast connection is not only dependent on the bandwidth available, but also on the feedback delay of the channel.The key idea of the HSDPA concept is to increase packet data throughput with methods known already from Global System for Mobile Communications (GSM)/Enhanced Data rates for Global Evolution (EDGE) standards, including *link adaptation* and fast physical layer (L1) retransmission combining[6]. In order to realize what it offers, HSDPA brings some changes like introduction of new channels, Hybrid ARQ and Adaptive modulation and coding. For the ARQ, inherent large delays of the existing Radio Network Controller based Automatic Repeat Request would result in unrealistic amounts of memory on the terminal side. Thus, architectural changes are needed to arrive at feasible memory requirements, as well as to bring the link adaptation closer to the air interface.

With HSDPA two of the most fundamental features of WCDMA, variable spreading factor and fast power control are disabled and replaced by adaptive modulation and coding (AMC), extensive multicode operation and a fast and spectrally efficient retransmission strategy. This basically means that terminal stores the received data packets in soft memory and if decoding has failed, the new transmission is combined with the old one before channel decoding. The retransmission can be either identical to the first transmission or contain different bits compared to the channel encoder output that was received during the last transmission. With this incremental redundancy strategy improved decoding efficiency and diversity gain can be achieved. In the next two chapters HARQ and AMC schemes are explained in more detail.

2.5.3.1 Hybrid ARQ

HARQ is a link adaptation scheme in which link layer acknowledgements are used for retransmission decisions in the UTRAN. In Release 99 retransmission functionality is part of the RLC layer. However, this kind of high-level retransmission scheme is too slow for the high-speed data transmissions envisaged for HSDPA. With HSDPA the HARQ retransmission buffers are located closer to the physical layer, specifically within the new MAC-hs logical entity that is just above the physical layer. The ARQ combining is based on incremental redundancy; that is, if a transmission fails, the received (corrupted) data is stored to a buffer. Successive retransmissions will include more redundancy, and they are combined with the old data in the buffer. This is repeated until the data in the buffer is considered to be correctly received, or the maximum number of retransmissions is reached. Also, here chase combining can be used. That is, the same packet is transmitted again and coherently combined with the previously received packet. Then it is decoded. In other words, this means that HARQ functionality is operated in two different ways. It is possible to send retransmissons (chase combining) or with different parameters, the transmissons will not be identical and then the principal of incremental redundancy is used. The latter method has a slightly better performance but it also needs more memory in the receiver, as the individual transmissons cannot be just added. At the highest data rate only soft combining may be used, while with lower data rates, also incremental redundancy can be used [6].

[5] UMTS Forum report 3G Offered Traffic Characteristics2 concludes that data traffic on downlink will exceed uplink traffic by a factor of 2:3.

2.5.3.2 Adaptive Modulation Coding (AMC)

Adaptive Modulation and Coding means that the shared channel transport format (i.e., the modulation scheme and the code rate) depends on the channel quality. This is monitored constantly, and the transport format used can be dynamically changed in every frame. The quality information is transmitted to the Node-Bs via the uplink control channels. That is, if the radio channel condition is good, the network can use higher-order modulation and less redundancy, whereas in poor conditions, a more robust modulation scheme can be employed and the data packets may have more redundancy in them. Release 5 employs two modulation schemes, namely QPSK and 16 Quadrature Amplitude Modulation (16QAM). Later releases may introduce other schemes, such as 64QAM.

CQI Number	Switch SINR (dB)	Modulation	Number of codes	Block Size
1	$-\infty$	QPSK	1	137
2	-2.475	QPSK	1	173
3	-1.075	QPSK	1	233
4	0.357	QPSK	1	317
5	1.275	QPSK	1	377
6	2.375	QPSK	1	461
7	3.525	QPSK	2	650
8	4.575	QPSK	2	792
9	5.425	QPSK	2	931
10	6.625	QPSK	3	1262
11	7.575	QPSK	3	1483
12	8.525	QPSK	3	1742
13	9.675	QPSK	4	2279
14	10.525	QPSK	4	2583
15	11.725	QPSK	5	3319
16	12.175	16QAM	5	3565
17	13.325	16QAM	5	4189
18	14.175	16QAM	5	4664
19	15.175	16QAM	5	5287
20	16.175	16QAM	5	5887
21	17.225	16QAM	5	6554
22	18.175	16QAM	5	7168
23	19.275	16QAM	7	9719
24	20.175	16QAM	8	11418
25	21.275	16QAM	10	14411
26	22.075	16QAM	12	17300
27	23.075	16QAM	15	21754
28	23.975	16QAM	15	23370
29	24.475	16QAM	15	24222
30	25.275	16QAM	15	25558

Table 2.2: AMC Modes

2.5.3.3 HSDPA Physical Layer Structure

To implement HSDPA three new channels are introduced in the physical layer specifications.

High Speed Downlink Shared Channel (HS-DSCH)

With the introduction of this channel, additional intelligence in the form of an HSDPA Medium Access Control (MAC) layer is installed in the Node B. This way, retransmissions can be controlled directly by the Node B, leading to faster retransmission and thus shorter delay with packet data operation when retransmissions are needed.

HS-DSCH has comparable characteristics with release '99 channels. The transmission time interval (TTI) is defined to be 2 ms. This is short compared to TTI lengths of release '99 and its purpose is to achieve short round trip delay for the operation between the node B and terminal for retransmissions and to allow "riding on the channel peaks" scheduling of users. From spreading code point of view spreading factor (SF) is fixed at 16 like before. The maximum number of codes that can be allocated is 15, but depending on the UE capability maximum number of codes a user can achieve are fixed at 5, 10 or 15.

Table 2.3 gives the comparison of the basic properties and components of HS-DSCH and DSCH.

Feature	DSCH	HS-DSCH
Variable Spreading Factor	Yes	No
Fast Power Control	Yes	No
Adaptive Modulation and Coding	No	Yes
Multicode operation	Yes	Yes, extended
Fast L1 HARQ	No	Yes

Table 2.3: Comparison of fundamental properties of DSCH and HS-DSCH

HS-DSCH Modulation: In HSDPA 16 QAM modulation was introduced in addition to Release '99 Quadrature Phase Shift Keying (QPSK). 16 QAM doubled the peak data rate compared to QPSK and allows up to 10 Mbps peak data rate with 15 codes of spreading factor 16. QPSK and 16 QAM constellation diagrams are given in figure 2.18.

HS-DSCH Channel Coding The major difference compared to the Release '99 is the addition of hybrid ARQ. When using QPSK Release '99 channel interleaver is used and when using 16 QAM, two parallel channel interleavers are applied. HSDPA capable Node B has the responsibility of selecting the transport format to be used g with the modulation and number of codes on the basis ofthe information available atthe Node B scheduler.

In case of 16 QAM constellation as in figure 2.18 different bits mapped to the 16 QAM symbols have different reliability. This is compensated with the ARQ proccess with the help of a method called *constellation rearrangement*. With this method different retransmissons use slightly differnent mapping of the bits to 16 QAM symbols. [6], [28]

High Speed Shared Control Channel (HS-SCCH)

This channel carries the physical layer control information necessary to decode HS-DSCH and performs the possible combination of data in case of retransmissions. Each HS-SCCH block is divided

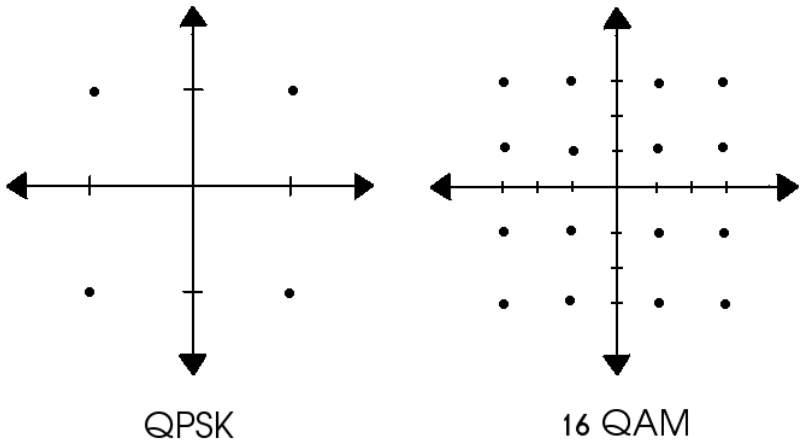

Figure 2.18: QPSK and 16 QAM constellations

into two functional parts.

Part 1 carries the following time critical parameters:

- Codes to despread. (also indicates UE capability)
- Modulation to indicate if QPSK or 16 QAM is used.

Part 2 parameters are less time critical ones and are listed as follows:

- redundancy version information to allow proper decoding and combining with the possible early transmissions.
- ARQ process number to show which ARQ process the data belongs to.
- First transmission or retransmission indicator to indicate whether the transmission is to be combined with the existing data in the buffer (if not successfully decoded earlier) or whether the buffer should be flushed and filled with new data.

Uplink High-Speed Dedicated Physical Control Channel (HS-DPCCH)

This channel carries the necessary control information in the uplink. Control information consists of ACK/NACK transmission to reflect the results of CRC and downlink channel quality indicator (CQI). In the addition of this channel, existing uplink channel structure was left unchanged and this channel was added in parallel. This is to ensure operation in soft handover in tha case that not all NodeBs have HSDPA capability.

HS-DPCCH carries the following information:

- ACK/NACK transmission, to reflect the results of CRC check after the packet decoding and combining.
- Downlink Channel Quality Indicator (CQI) to indicate which estimated transport block size, modulation type and number of parallel codes could be received correctly in the DL direction.

The above mentioned feedback information consists of 5 bits and carry quality related information. One signaling state is reserved for the state “do not bother to transmit” and other states represent the transmisson that the terminal can receive at the current time.

The HS-DPCHH needs some part of the uplink transmisson power, which has an impact on the link budget for the uplink.

Figure 2.19 gives a visualisation of the new channels added for HSDPA.

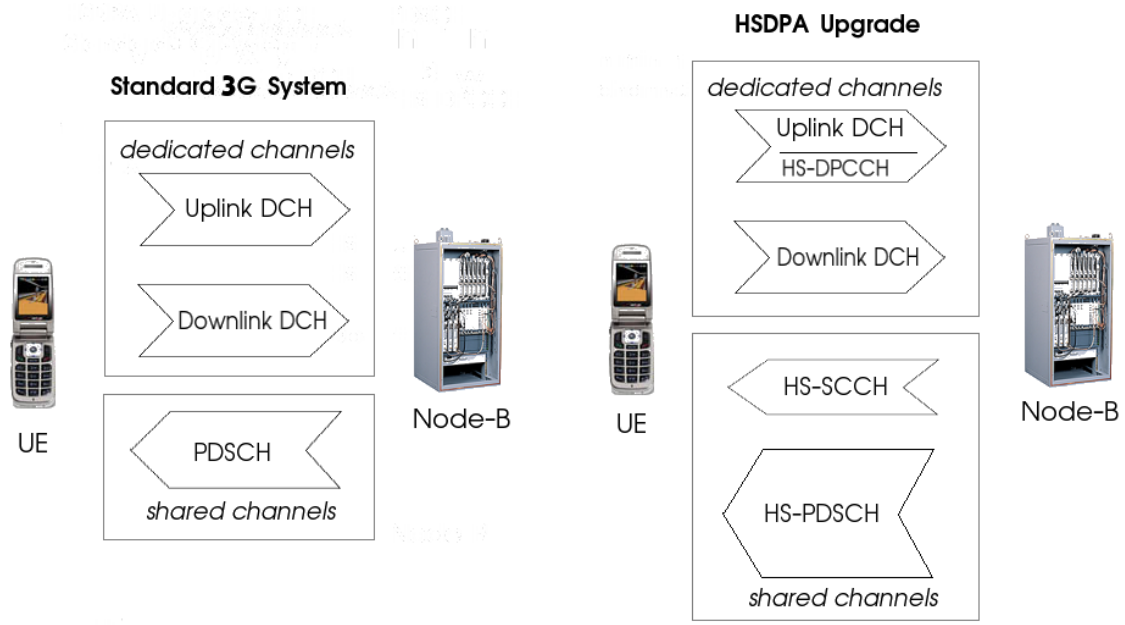

Figure 2.19: HSDPA Upgrade

2.5.3.4 HSDPA Terminal Capability and Achievable Data Rates

In HSDPA there are 12 possible optional terminals with varying maximum data rates between 0.9 and 14.4 Mbps. The differences between the classes lie in the maximum number of parallel codes that must be supported and whether the reception in every 2 ms TTI is required.

2.5.4 Factors Governing HSDPA Performance

Time dispersion, cell environment, terminal velocity as well as experienced own cell interference to other cell interference ratio effect the performance of an HSDPA system. Also from the mobile side, basic detector performance and HSDPA capability level 2.4 is effective. Also, it is important how the radio resource management is done. That is, power and code resources allocated to HSDPA channel, accuracy of signal to interference power ratio and packet scheduling algorithms. Especially, packet scheduling algorithm is very important when extension to MIMO systems is in consideration.

From the other side, in addition to the more system level effective factors of the previous paragraph, single user link adaptation performance depends on some other additional issues. Such as CQI measurement, transmission and processing delays 2.2.1. This adds to the inherent delay associated with the two slot time difference between the HS-SCCH frame and the corresponding HS-DSCH packet. The minimum total delay is 6 ms between the time of estimation of the CQI report and the time when the first packet based on this report can be received by the UE. (The target BLER for CQI report is 10%) [6].

Category	Maximum nr. of parallel codes HS-DSCH	Minimum inter-TTI interval	Transport channel bits per TTI	ARQ type at max data rate	Achievable maximum data rate (Mbps)
1	5	3	7298	Soft	1.2
2	5	3	7298	IR	1.2
3	5	2	7298	Soft	1.8
4	5	2	7298	IR	1.8
5	5	1	7298	Soft	3.6
6	5	1	7298	IR	3.6
7	10	1	14411	Soft	7.2
8	10	1	14411	IR	7.2
9	15	1	20251	Soft	10.2
10	15	1	27952	IR	14.4
11	5	2	3630	Soft	0.9
12	5	1	3630	Soft	1.8

Table 2.4: HSDPA Terminal Capability Categories

2.5.5 Link Level in Simulator

As discussed in chapters 2.5.3.2 and 2.5.3.1 the mapping from SNR to system throughput depends on applied ARQ scheme, the selected AMC mode and the number of codes that were used. This selection is made based on the CQI report from the mobile. In table 2.2 it can be seen that, a direct mapping petween SNR values and CQI is possible. In the simulations link-level results from analytical investigations (Figure 2.20) have been used with an approach for the derivation of the SNR-throughput mapping presented in [29].

In order to make it more clear how this mapping works consider that at a particular TTI time, channel quality reported to the NodeB is equivalent to an SINR of 14.5 dB. According to the table 2.2 this value is assigned to a CQI of 18 and associated graph of this value from figure 2.20 is plotted as solid blue line in figure 2.21. Here it can be seen that this SINR value can reach at most 2.332 Mbps throughput in case the reported delay is completely right. However aim of this mapping is to reflect the effect of variable feedback delay to system throughput. Again according to figure 2.21, if actual SINR value at that particular TTI is not as high as 14.5 dB, say for example 12 dB then system will have 1.166 Mbps. From the other side, reported feedback value may be less than the actual. In that case, say for example at 16 dB system can in fact reach up to 2.643 Mbps, while due to the pesimistic ARQ scheme, AMC mode and/or code number choice system stays at 2.332 Mbps which is again a degradation of performance due to out-dated channel quality information arising from feedback delay.

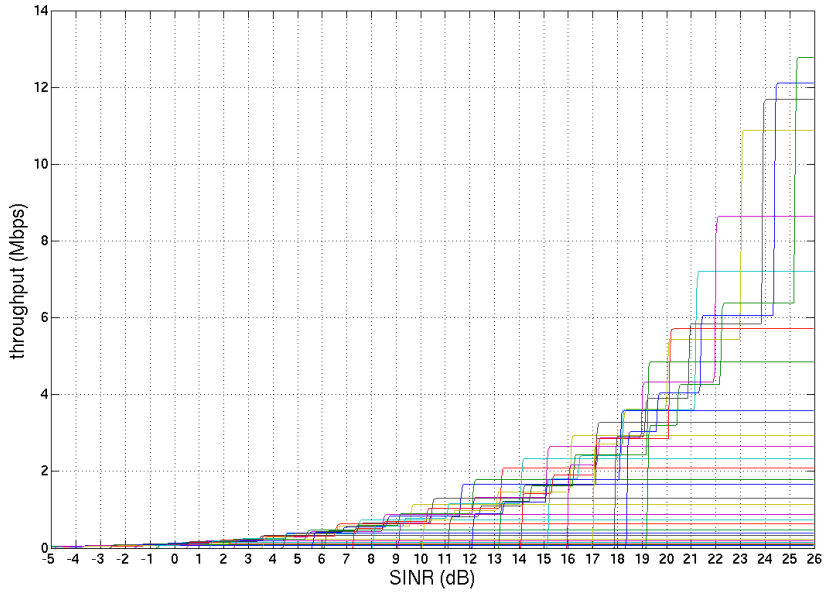

Figure 2.20: HSDPA Link level results from analytical investigations.

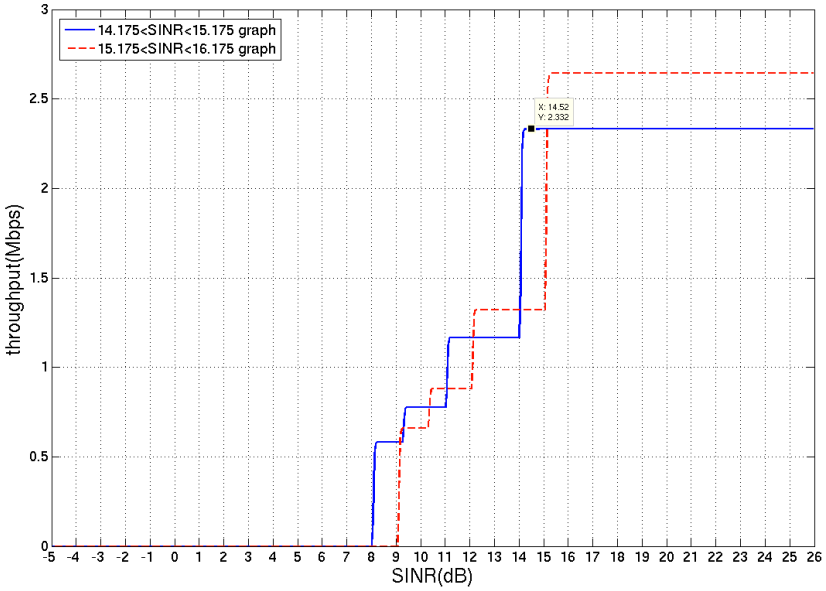

Figure 2.21: HSDPA Link level results from analytical investigations (for reported SINR values from 14.175 to 16.175).

3 Scenario

This chapter presents the scenario that is used in the simulations. Simulator assumes an outdoor cell that has a diameter of 2000 m as shown in figure 3.1. In this cell random positioned users are created each having a particular *user distance*, *direction of arrival (DOA)*, *direction of departure (DOD)*, *direction of arrival spread (DOA spread)* and *direction of departure spread (DOD Spread)* and each moving at a predefined speed.

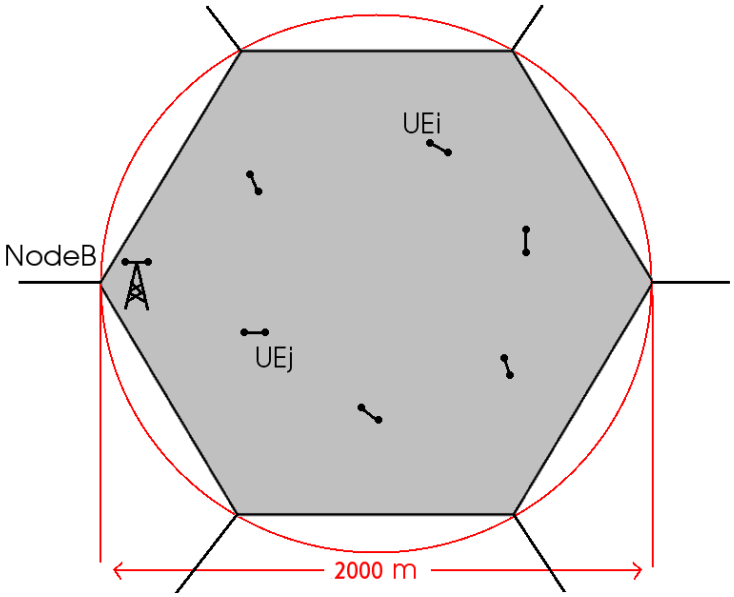

Figure 3.1: Shape of the simulated cell and some randomly distributed users inside the cell

Together with the antenna separation values in terms of carrier wavelength λ, these are the parameters required for defining the scatterer distribution and hence spatial correlation matrices. In the simulator, two scatterer distribution types are possible, namely uniform and laplacian.

Taking into account the link level channel model parameters given in [25] above mentioned parameters have the following values if not otherwise stated.

For the number of antennas the most interesting pairs are 2×2 case and 4×2 case. To use more than 2 antennas at the receiver side is not very realizable due to the small size of the mobiles. For the base station side 2 or 4 antenna assumption is more realizable with respect to higher number of antennas as required space and cost becomes an issue. Figure 3.2 shows the definition of the parameters of table 3.1 using a similar approach as was assumed in figure 2.12. Although two sides are drawn as independent systems, superposition of the two sides should be considered.

Figure 3.3 shows the azimuth pdf of the mobile side for the laplacian scatterer distribution as given in equation 2.57. $\zeta = 35$ degrees and θ is defined for $\pm 3\zeta$. Also note that $\phi_0 = 0$ in the figure.

Figure 3.4 gives the azimuth pdf for the BS side for $\zeta = 5$ degrees and θ is defined for $\pm 3\zeta$ again for $\phi_0 = 0$. Also polar plots are given for easy visualization next to each figure.

Parameter	Value
user distance	$0 \leq dist \leq 2000m$
DOA	$-60 \leq DOA \leq 60$
DOD	$-90 \leq DOD \leq 90$
DOA Spread Deg.	5
DOD Spread Deg.	35
RX antenna separation	2λ
TX antenna separation	15λ

Table 3.1: Link Level Channel Model Parameters

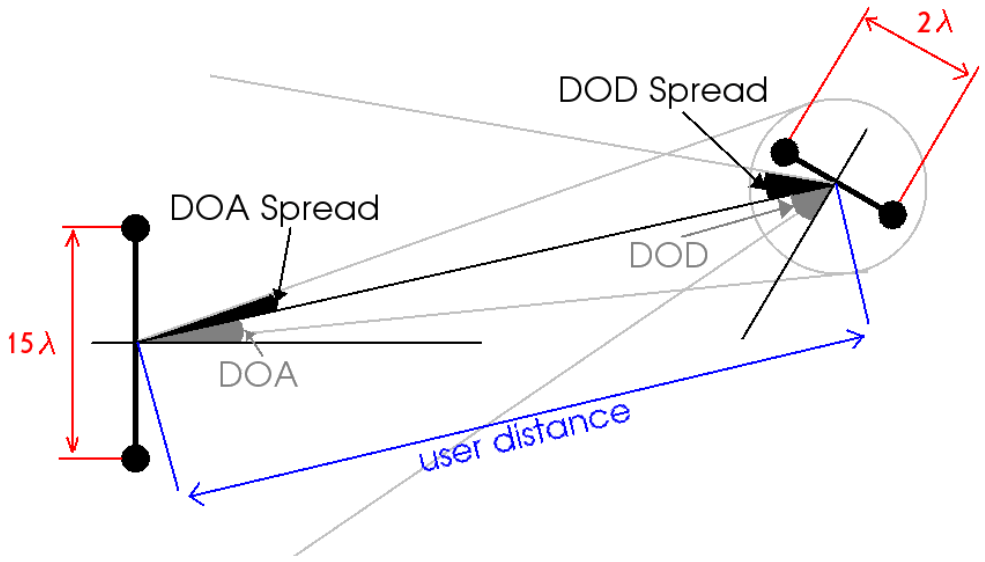

Figure 3.2: Link Level Channel Model Parameters

Other parameters from the table 3.1 to be discussed about are BS and MS antenna separations. These parameters are effective for *angular resolvability* of the MIMO system and hence the well-conditionedness of $\boldsymbol{H}$ so that additional degrees of freedom coming from MIMO structure can be used to increase the capacity [1].

A common pictorial representation of the angular resolvability of an antenna array is the (receive) *beamforming pattern*. Figure 3.5 gives a pictorial representation of the beamforming patterns of BS side and MS side for 2×2 case. Antenna separations are 2λ and 15λ for MS side and BS side respectively. However, note also that in order to represent a cellular structure as given in figure 3.1 with base station located at the left side of the hexagon, such an omnidirectional pattern is not enough. In order to include this effect sectorization gain of the base station antenna array should also be added to channel. Sectorization gain pattern used in simulation scenarios is plotted in figure 3.6. Note that sectorization gain goes down to -3dB at $\pm 35^\circ$ which corresponds to a beam width of 70°. Also if the cell boundaries are assumed to be $\pm 60^\circ$ it can be seen that at those angles sectorization gain goes down to -10 dB.

Another important parameter about the simulation scenarios is the total transmit power of the base station. Value of this power is taken as 20W. However note that only 80% of this power is given to HS-DSCH channels. Rest is used for shared channels (i.e. control or pilot channels).

On the other side of the channel, at the mobile side noise power is taken to be -99dBm inside of which

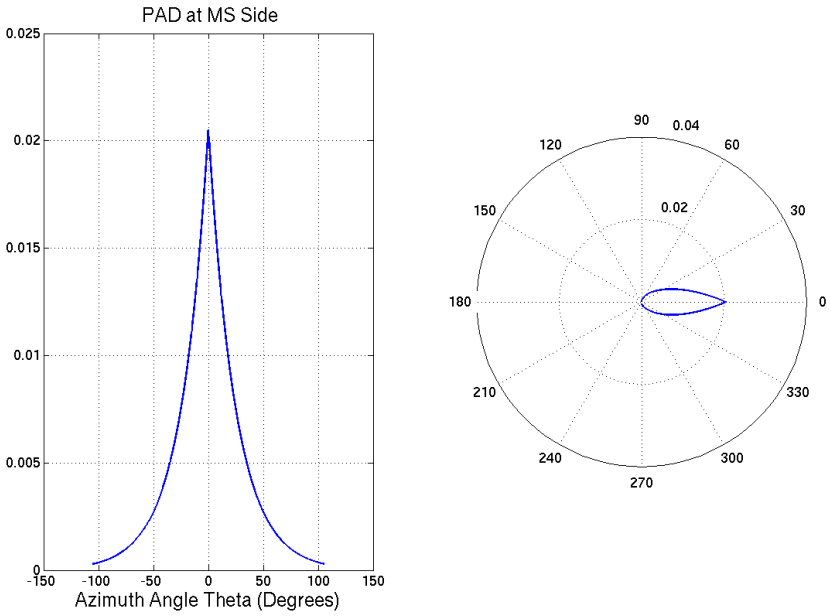

Figure 3.3: Azimuth pdf for MS side (Laplacian)

noise coming from the analog front end of the mobile is 9 dB. A summary of those mentioned in this chapter and some other important scenario parameters can be found in table 3.2.

Parameter	**Value**
Cell radius	1000m
Sectorization Pattern	$-10dB \quad at \quad 60^{\circ}$
User Placement	Uniform in cartesian coordinates
Total Transmit Power	20W
Path Loss Exponent	3.76
Power Portion of HS-DSCH	80 %
Antenna Gain	17 dBi
Orthogonality Factor	0.1
Shadowing Correlation btw. S and $I_{intercell}$	50%
Noise Power	-99dBm
MS Power Angular Density	Laplacian, Uniform
BS Power Angular Density	Laplacian, Uniform

Table 3.2: Link Level Channel Model Parameters

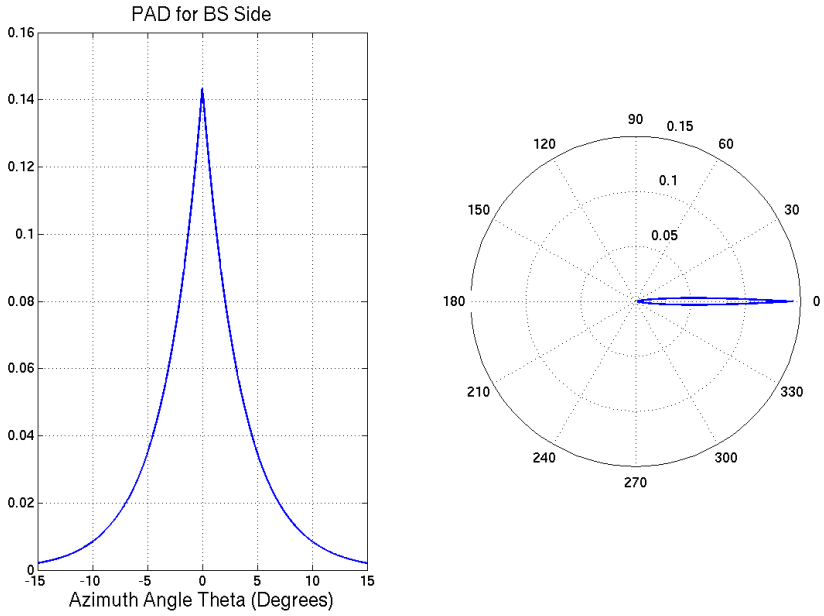

Figure 3.4: Azimuth pdf for BS side (Laplacian)

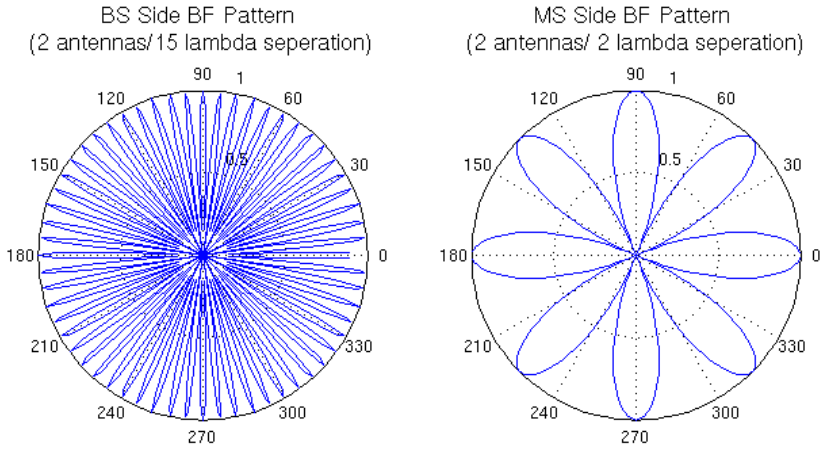

Figure 3.5: MS and BS beamforming patterns for a 2×2 system. Antenna separations are 2λ and 15λ respectively

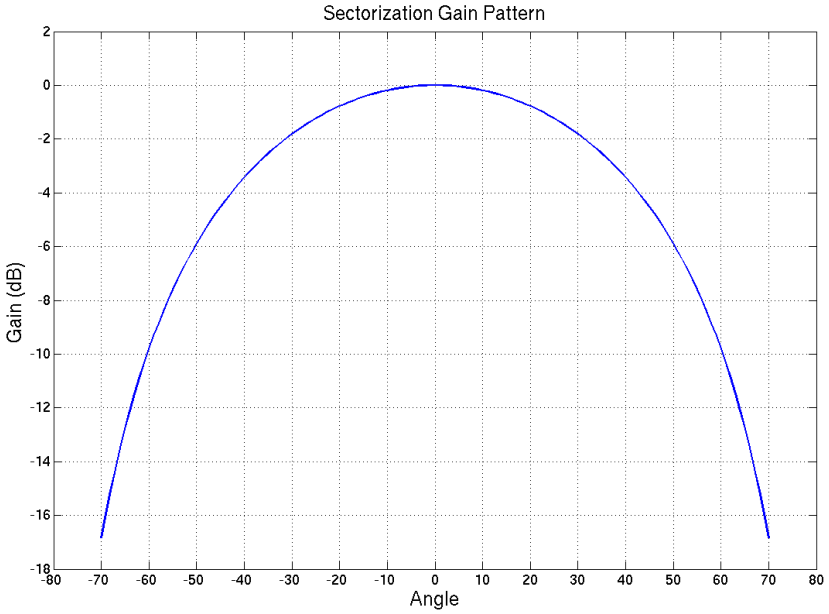

Figure 3.6: Sectorization Gain Pattern

4 Results and Discussions

In chapter 2.3, some approaches for creating weight vectors for opportunistic beamforming for MISO case were discussed and in 2.4.7 another approach inspired from SVD decomposition of a MIMO channel. This chapter begins by comparing two main opportunistic beam-forming techniques that were focused on. Namely *channel SVD beam forming approach* based on 2.4.7 and *MIMO phase shift beam-forming approach* based on 2.4.6.

4.1 Comparison of Beamforming Approaches

4.1.1 Relation of Channel SVD Beam-forming Approach and MIMO Phase Shift Beam-forming Approach

In order to have more meaningful graphs in the following chapters the first thing that should be investigated is the relation of the two approaches that were discussed in the previous chapters. Both of them aim to increase channel fluctuation in a controllable way to exploit multiuser diversity as much as possible but one of them has $\Delta\theta$ as design parameter while the other one has the corresponding changing speed.

This problem can be approached as follows. Auto-correlation functions of the weight vectors applied to a specific data stream are computed. These vectors are nothing but a column of matrix $\boldsymbol{W}$. Then a reasonable match between an auto-correlation from the channel SVD beam forming approach for a specific speed and an auto-correlation from the MIMO phase shift beam-forming approach for a specific $\Delta\theta$ is tried to be found.

Consider the following $\boldsymbol{W}$ matrix

$$\boldsymbol{W}[m] = \begin{bmatrix} w_{11}[m] & w_{12}[m] \\ w_{21}[m] & w_{22}[m] \end{bmatrix} \tag{4.1}$$

Then the autocorrelation function $\boldsymbol{R}(\tau)$ would be for any of the two streams

$$\mathbb{R}(\tau) = \sum_{n=-\infty}^{\infty} \begin{bmatrix} w_{1i}[m] & w_{2i}[m] \end{bmatrix} \begin{bmatrix} w_{1i}[m-\tau] & w_{2i}[m-\tau] \end{bmatrix}^H \tag{4.2}$$

Figure 4.1 shows how does the autocorrelation of the weight vector applied to one stream looks like. Note that as the equivalent speed increases, peak of the autocorrelation graph narrows. That is expected since we decrease the correlation as we introduce faster changing weight matrices to the effective channel. Similarly autocorrelation of the weight vector applied to one stream in phase shift approach looks like in figure 4.2.

First attempt will be to define a rule of thumb for the relation of two different approaches according to the spread of autocorrelation graphs. Then an attempt to confirm this rule of thumb will be made by taking a look at the mean squared error powers. The reason why MSE values are also interesting

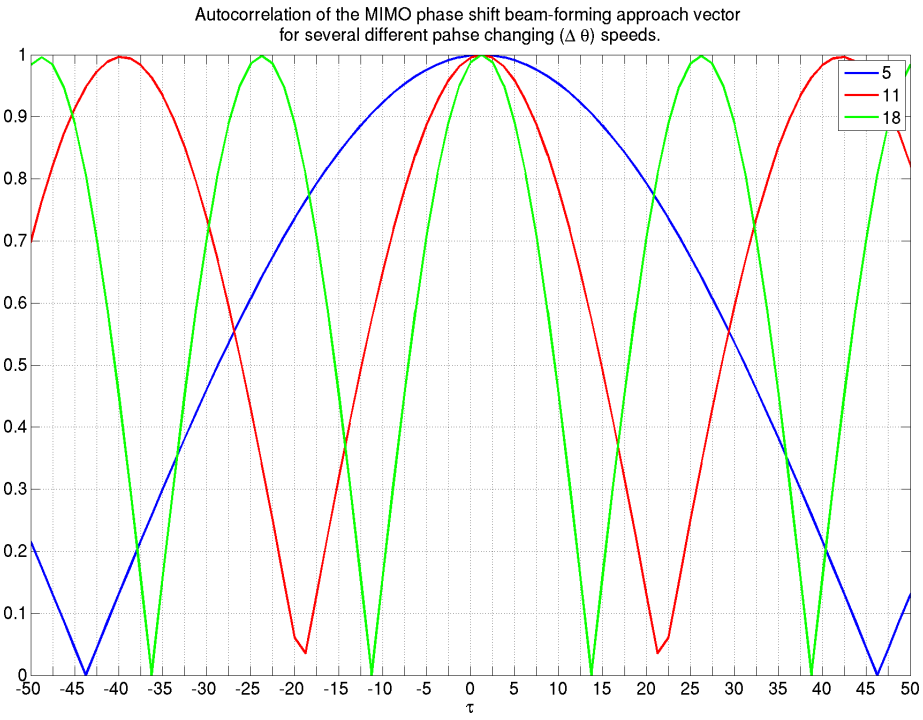

Figure 4.1: Autocorrelation of a single weight vector applied to one of the streams under several different equivalent speeds.

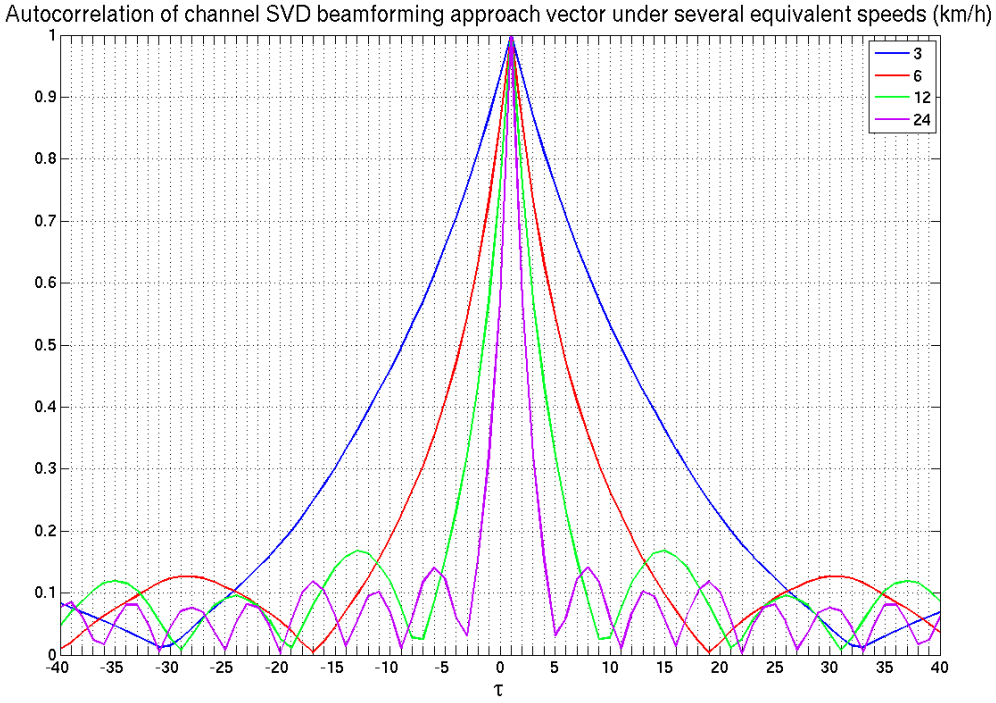

Figure 4.2: Autocorrelation of a single weight vector applied to one of the streams under several different $\Delta\theta$ values

is discussed at chapter 2.2.1. Figure 4.3 shows that the spread, hence the temporal correlation of the applied $\boldsymbol{W}$ matrices decreases with the increasing equivalent speed or increasing $\Delta\theta$. Note also that, main lobe of the channel SVD beam forming approach is sharper than phase shift approach. That is why in figure 4.3 right side decreases faster. Actually, because of this reason it is not easy to say directly that a $\Delta\theta$ value (10 degrees in 4.3) that causes the same spread (17 τ in 4.3) as an equivalent speed value (6km/h in 4.3) is totally equivalent to it. But nevertheless, this is a good way to approach the problem and will be taken as a rule of thumb. In fact, below it turns out to be a very good estimate.

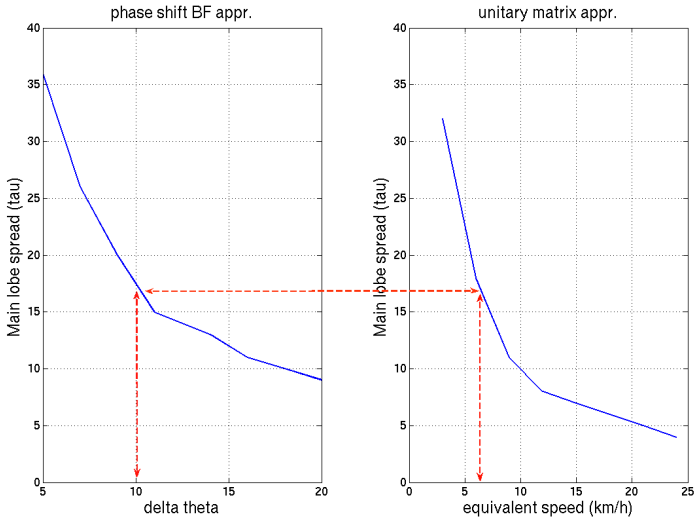

Figure 4.3: Spread of autocorrelation graphs for two different approaches.

Keeping in mind figure 4.3 two specific cases will be focused on. For the phase shift beamforming approach $\Delta\theta = 10$ degrees and for channel SVD beam forming approach case an equivalent speed of 6km/h is used for unitary matrix creation. In chapter 2.2.1 it was discussed that feedback delay becomes an important issue as the channel fluctuation increases. Due to the delay there will be an error in feedback information of channel quality. Actually mean square value of this error is dependent on the channel fluctuation rate and should be same for channels that fluctuate at the same speed. Here also note that in the previous cases $\boldsymbol{W}$ matrices were considered and channel was not taken into account. But MSE arising from the feedback delay is completely a channel observation result and effects scheduler and therefore system throughput directly. Figure 4.4 shows that actually matching choice according to 4.3 produces nearly same MSE performance under same feedback delay (2 TTI) conditions. In order to demonstrate that the MSE would be different for two random points in figure 4.3 (i.e not horizontally at the same τ value) the figure 4.6 is also presented.

4.2 Predictor Performance

In chapter 4.1 equivalence of two beamforming approaches is discussed for a meaningful comparison. This chapter focuses on the error performance of the RLS estimator that was discussed on chapter 2.2.3. Error performance is investigated by looking at the mean squared error values.

Any adaptive filter has a convergence time in which coefficients are adapted to the current signal to be estimated. In RLS filter this value should be in the order of $1/(1-\lambda)$ where λ is called the *forgetting factor* and taken as 0.99[1]. A training period is assumed during which adaptive RLS filter should converge to the signal to be estimated. During the training period the real value of the signal

[1] See Appendix A.3

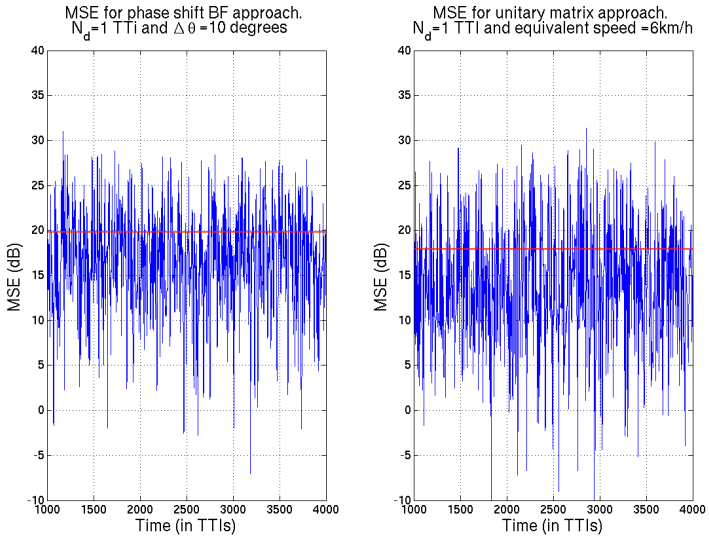

Figure 4.4: MSE performance according to proposed rule of thumb.

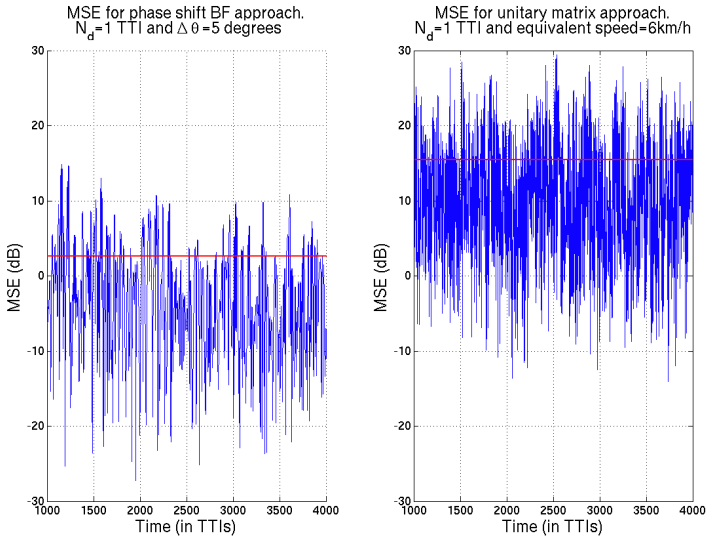

Figure 4.5: MSE performance of random $\Delta\theta$ and equivalent speed values that cause different auto-correlation spreads.

is known and hence stabilized RLS algorithm presented in 2.1 can be applied. That is, coefficients are updated at each TTI during this period. Training period is taken to be 2000 TTIs (4 sec) in the following graphs if RLS estimator is used.

Apart from the above, the most important parameter that should be optimized in the RLS adaptive filter is the size of $\boldsymbol{w}(t)$ or the number of filter coefficients. Filter coefficients directly effect the precision of the estimator and processing power required. Figure 4.6 shows the MSE performance of the same RLS filter under the conditions discussed in chapter 4.1. It can be seen that After 6 coefficients towards 10 coefficients error performance tends to saturate and also processing power required for the calculations increases. Hence, more than 10 filter coefficients is not very interesting.

Another clear observation in figure 4.6 is that, MIMO phase shift beamforming approach is always more predictable (from MSE point of view) with respect to channel SVD beamforming approach. Note that this is also intuitive since in phase shift beamforming approach, dynamics that we introduce

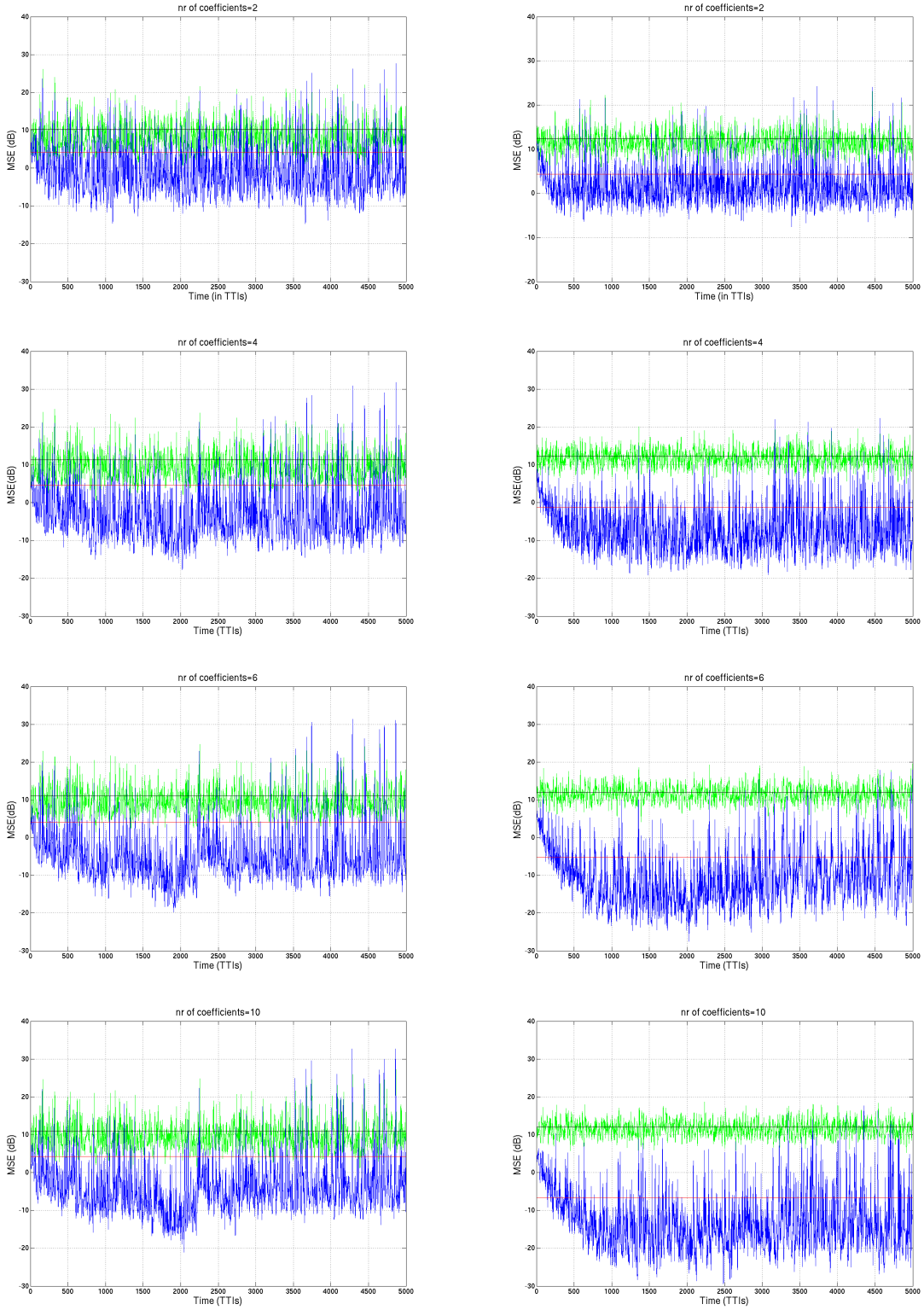

Figure 4.6: MSE performance of channel SVD beam forming approach at 4km/h equivalent speed (left) and phase shift beamforming approach at 8 degree $\Delta\theta$ (right)

to the channel is periodic, while in channel SVD beamforming approach a virtual fast fading profile is assumed and if necessary sampled which is a more random process (sharp peak in 4.2). This fact already makes phase shift beamforming approach more interesting compared to channel SVD beamforming approach. Moreover, even if we assume that there is no feedback delay and hence no

need for an estimator, simulation results in figure 4.7 show that phase shift beamforming approach performs better than channel SVD beamforming approach. Because of these facts we will focus on the first technique in next chapters.

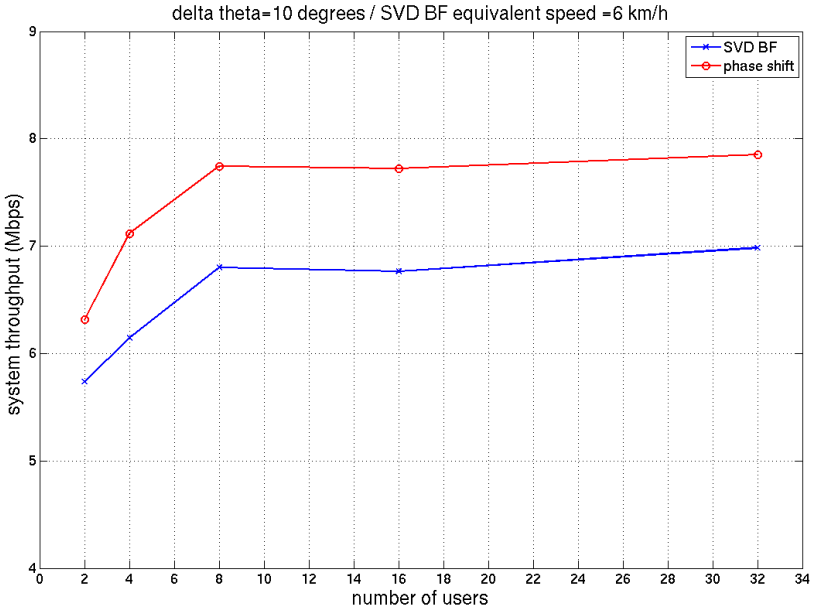

Figure 4.7: Comparison of Phase Shift Beam-forming Approach and Channel SVD Beam-forming Approach under corresponding conditions as discussed in 4.1

4.3 System Throughput Results (wrt T_c)

In the proportional fair scheduler, time constant T_c is also an important parameter that has an effect on overall system performance. T_c defines the time window that the averaging is made upon, hence larger T_c makes better exploiting of multiuser diversity available. But it also defines roughly the time a user may not be scheduled, hence very large values may not be desirable from QoS point of view.

Figure 4.8 shows that, for smaller values of T_c opportunistic beamforming is more effective. This is because for a channel without opportunistic beamforming, average number of fluctuations in that time window decreases as we decrease T_c and the relative dynamics that opportunistic beamforming brings in that time window is higher for smaller T_c values.

4.4 System Throughput Results (wrt $\Delta\theta$)

As discussed in chapter 2.4.6 $\Delta\theta$ is the parameter that controls the level of fluctuation that phase shift beamforming introduces in the channel. In case of no feedback delay the faster we apply opportunistic beamforming the better our gain will be and will saturate in the end. But in reality there will be a feedback delay which makes the optimization of $\Delta\theta$ necessary. Figure 4.9 shows that in case of feedback delay increasing theta increases the system throughput up to a point and then begins to fall down because error in channel quality feedback information increases. And figure 4.9 also shows that in case of estimator we can slow down the rate of decrease wrt $\Delta\theta$ but nevertheless estimator will also be affected from very high $\Delta\theta$ values negatively. It should also be noted that increasing $\Delta\theta$ for higher and higher values does not actually mean that effective dynamics introduced to the channel

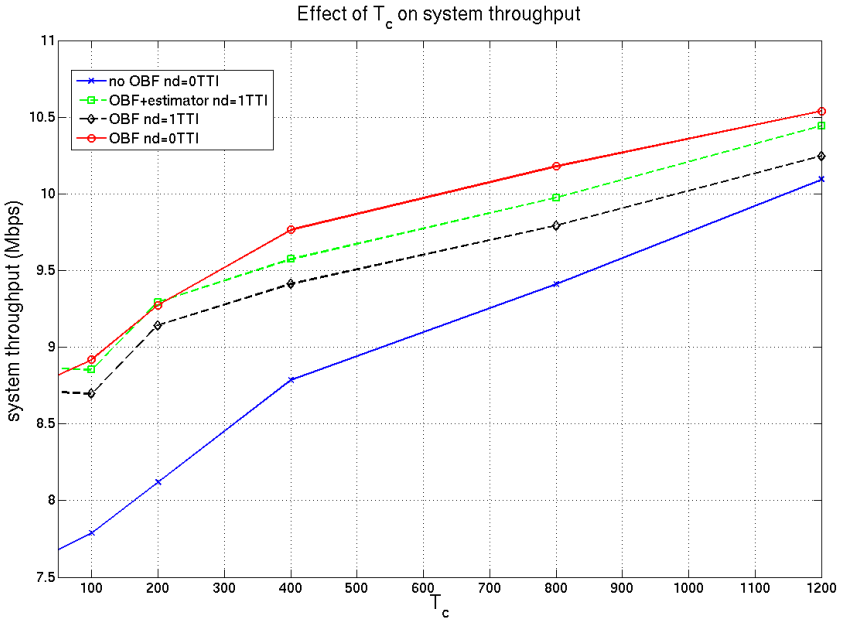

Figure 4.8: Effect of scheduler time constant T_c on system throughput for 10 users

will increase proportionally. Actually, in figure 4.9 in case of no feedback delay this is the reason why we have some decrease after 20 degrees and 24 degrees of θ increment performs close to 12 degrees.

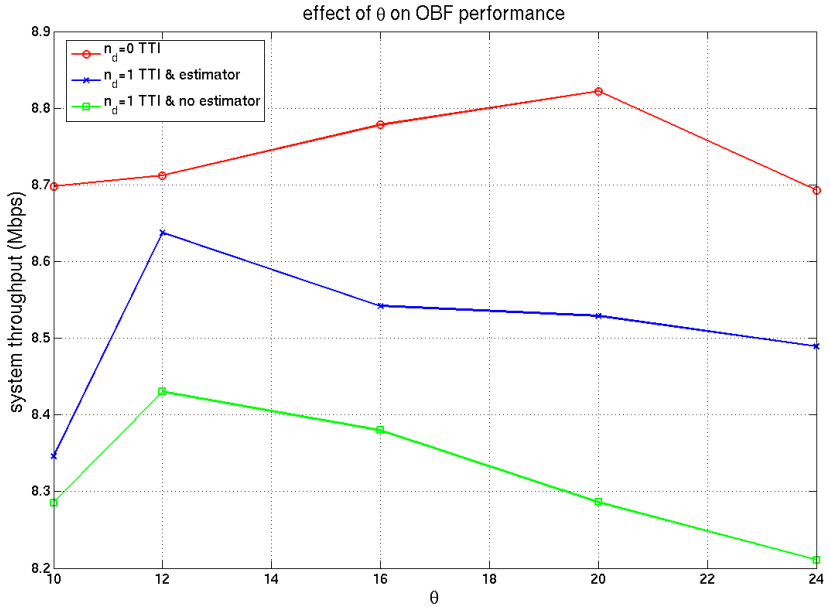

Figure 4.9: Effect of θ on opportunistic beamforming performance with and without estimator.

4.5 System Throughput Results (wrt Number of Users)

Figure 4.10 gives the system throughput performance for MIMO phase shift beamforming with $\Delta\theta =$ 12 degrees and an MMSE receiver at the UE side is used. It is assumed that there is no feedback delay.

Note that for 0 feedback delay 20 degrees would actually be the optimum value according to 4.9, but for comparison purposes with the other graphs where there is some feedback delay 12 degrees is used, and the speed of the users in the cell is 0.5 km/h.

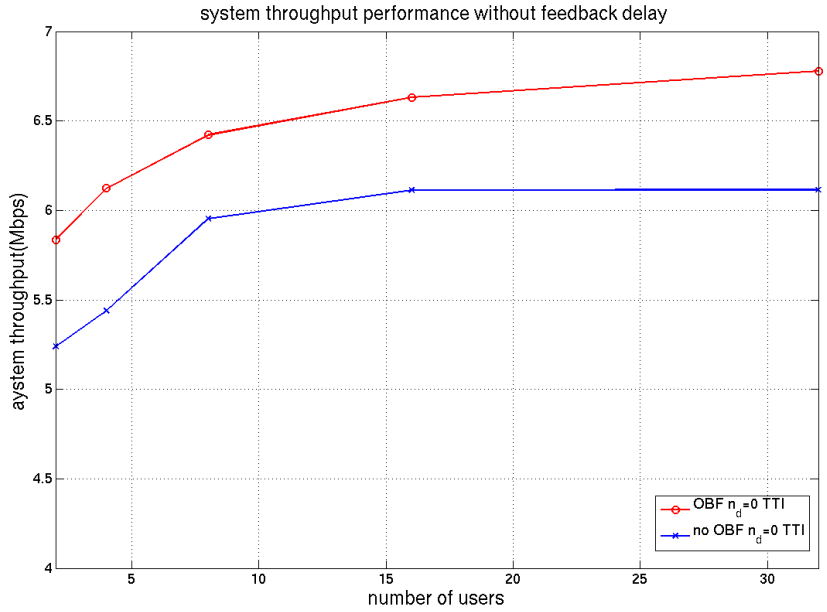

Figure 4.10: Opportunistic beamforming gain

Figure 4.10 assumed 0 feedback delay. In figure 4.11 system throughput decrease in case of feedback delay of 1 TTI is given for opportunistic beamforming case. It is also shown that for a feedback delay of 1 TTI application of an estimator can almost completely remove the performance decrease.

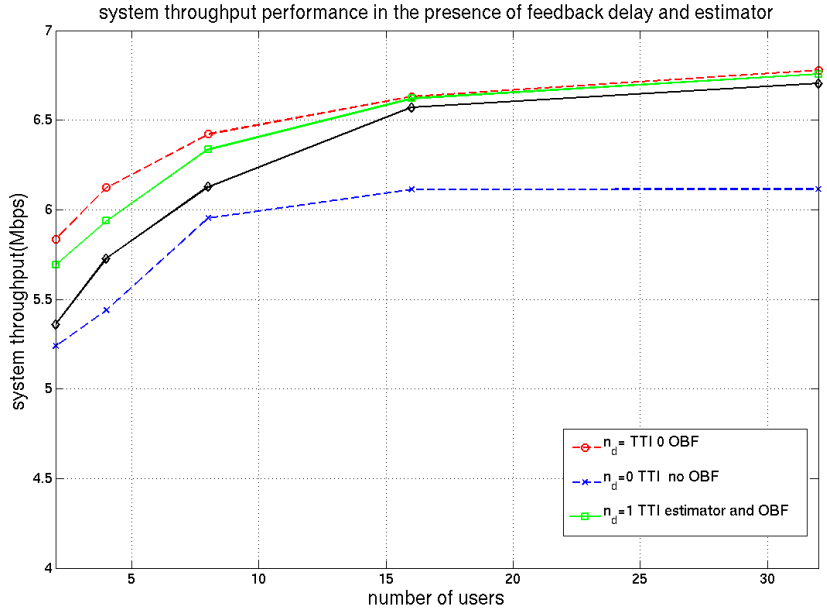

Figure 4.11: Effect of feedback delay and estimator usage

Figures 4.10 and 4.11 assumed users moving at a speed of 0.5 km/h and opportunistic beamforming parameter $\Delta\theta$ was 12 degrees. Also feedback delay of 1 TTI is taken if necessary. Effect of change

in value of any of these parameters are also of interest and figures 4.13, 4.12, 4.15, 4.14 are given to demonstrate the conditions of 2 or 3 TTIs feedback delay and in case of users moving at 3km/h.

In figures 4.12 and 4.14 it can be seen that feedback delay effect is more severe under opportunistic beamforming since channel dynamics is higher and in fact in case of no estimator, opportunistic BF application can even decrease the performance. This is nothing but the effect that was discussed in chapter 2.2.1 and showed with figure 2.5.

In figure 4.13 effect of RLS estimator under 2TTIs of feedback delay is demonstrated. It can again be seen that estimator can increase the system throughput. In this figure an RLS estimator with 10 coefficients is used and it should be noted that gain of RLS estimator is closely dependent on $\Delta\theta$. It gets easier for the estimator to match the signal if its rate of fluctuation is low while from the other side it can be roughly said that smaller $\Delta\theta$ values decrease the opportunistic beamforming gain as was discussed in chapter 4.4 . It is an optimization problem that depends on the channel properties to choose a suitable $\Delta\theta$. Figure 4.15 shows the estimator performace as the feedback delay increases to 3TTIs. Here estimator gain is even more than the case of 2 TTI feedback delay.

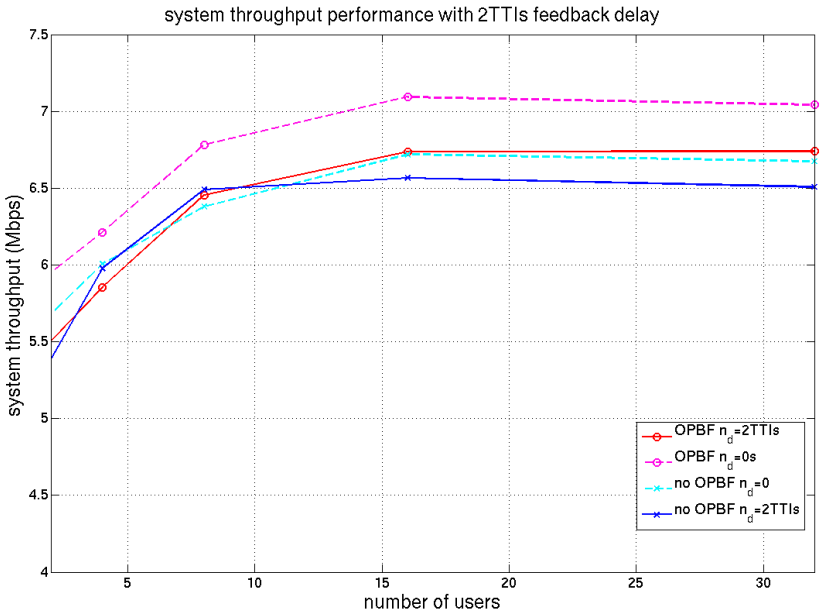

Figure 4.12: Effect of feedback delay of 2 TTIs with and without opportunistic beamforming

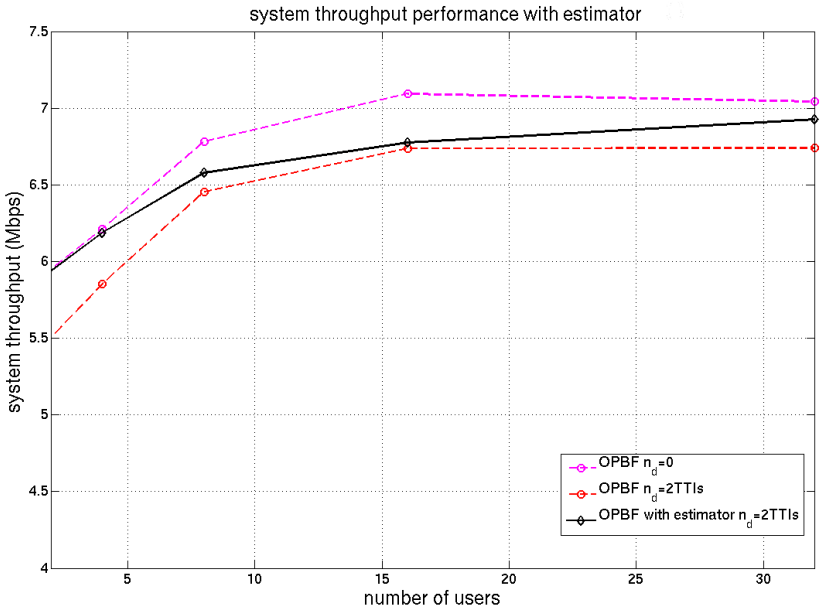

Figure 4.13: Effect of estimator in case of 2 TTIs feedback delay

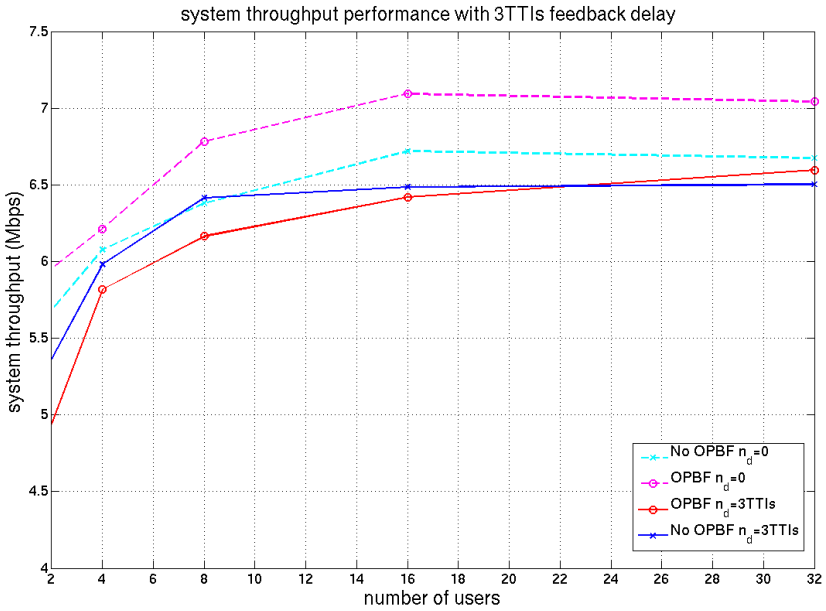

Figure 4.14: Effect of feedback delay of 3 TTIs with and without opportunistic beamforming

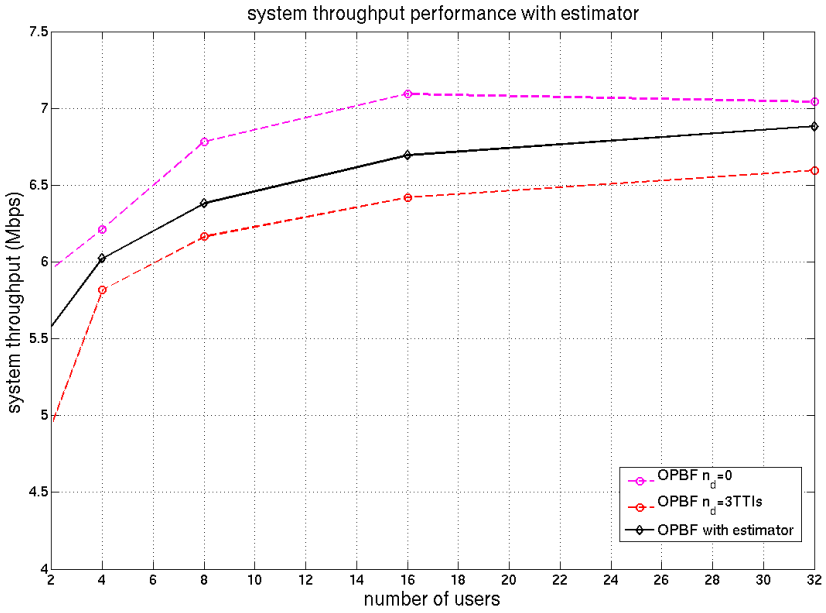

Figure 4.15: Effect of estimator in case of 3 TTIs feedback delay

5 Conclusions and Outlook

Within this thesis opportunistic beamforming idea was considered together with a MIMO wireless communication system, specifically HSDPA. MIMO extensions of already existing MISO opportunistic beamforming algorithms and new approaches that arise from the nature of the MIMO channel are investigated. An algorithm that is basically an extension of the MISO phase shift beamforming approach and an algorithm that arises from the resolvability of a MIMO system into parallel pipes using singular value decomposition are compared.

Comparison was made considering as much side effects as possible that are encountered in real wireless systems and degrades the system performance. SINR derivations are made considering interstream interference, intercell interference, multipath interference, intracell interference and noise in the channel. Also, non-feedback delay cases were considered which is essential for obtaining realistic results.

It is found out that, feedback delay effects the precision of channel quality report that is sent back to the basestation. Therefore a system throughput decrease that is directly related to the duration of the feedback delay is observed. In order to decrease the effect of feedback delay and considering the correct channel quality report is actually a shifted version of the current channel quality report, idea of applying an RLS estimator was proposed.

Considering the side effects and the performance of the RLS receiver for the two different beamforming approaches, it turned out that MIMO phase shift beamforming approach brings more promising results with respect to the case based on singular value decomposition of the channel.

After that focus is given on the analysis of the MIMO phase shift beamforming approach with respect to several different parameters. One of the main parameters that effects the performance of the opportunistic beamforming is the speed of the fluctuations that are introduced to the channel with opportunistic beamforming. It was shown that, at the presence of feedback delay, increasing channel dynamics via opportunistic beamforming can make the performance even worse if parameters of the opportunistic beamforming are not chosen carefully. When feedback delay is considered to be ideally 0 it may not be an issue but in fact it was seen that this is a very optimistic assumption and actually speed of opportunistic beamforming is an optimization problem.

This optimization differs from scenario to scenario. For example, it is important if estimator is used, how much feedback delay does the channel have, how many antennas does the MIMO system have at the transmitter and receiver side, how many users are in the cell, how fast they are etc.

While effect of all the above theoretical and practical parameters on the capacity are converted into throughput values, an HSDPA system is assumed. Analytical investigation results from the real HSDPA systems are used for the translation of the capacity into throughput, so that imperfections in the choice of applied ARQ scheme, the AMC mode and the number of codes that were used are directly projected on the system performance.

A Appendix

A.1 Separability of pipes in the proportional fair scheduler

In case of MIMO system users in the cell feed back the channel quality information for each stream. For example, for a 2×2 system this means a UE sends 2 seperate feedback signals indicating the quality of the channel. Here it is important how the proportional fair scheduler in the base station will use these parallel signals. Simulations of chapter 4 assumed that a basestation can schedule different mobiles for different pipes. That means during the same TTI one pipe may be reserved for one user while the other pipe is sent to another user.

From implementation point of view it may also be interesting to schedule only one user at a TTI. In that case parallel feedback information may be added to make a decision and only one user is scheduled using all the pipes at a TTI. Obviously a performance degradation will be experienced in this case since we are practically decreasing the level of diversity. Figure **??** shows the performance decrease wrt number of users without any opportunistic beamforming applied and moving at 3km/h.

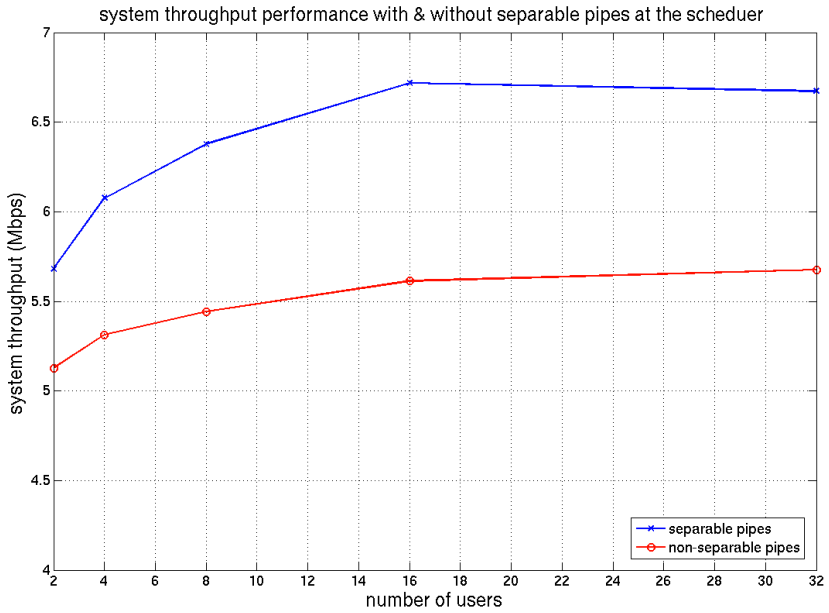

Figure A.1: Relative system performance example for case of separable and non-separable pipes

A.2 Zero Forcing Receiver Performance

In chapter 4 all the simulation results presented used MMSE receiver. In chapter 2.4.4 zero forcing receiver was also mentioned and its SINR equation was derived for a MIMO system which is a simpler

receiver and performs comparable to MMSE receiver especially at high SNR values. Figure A.2 gives the averall system performance in case of 0 feedback error and MMSE performance is also given for comparison.

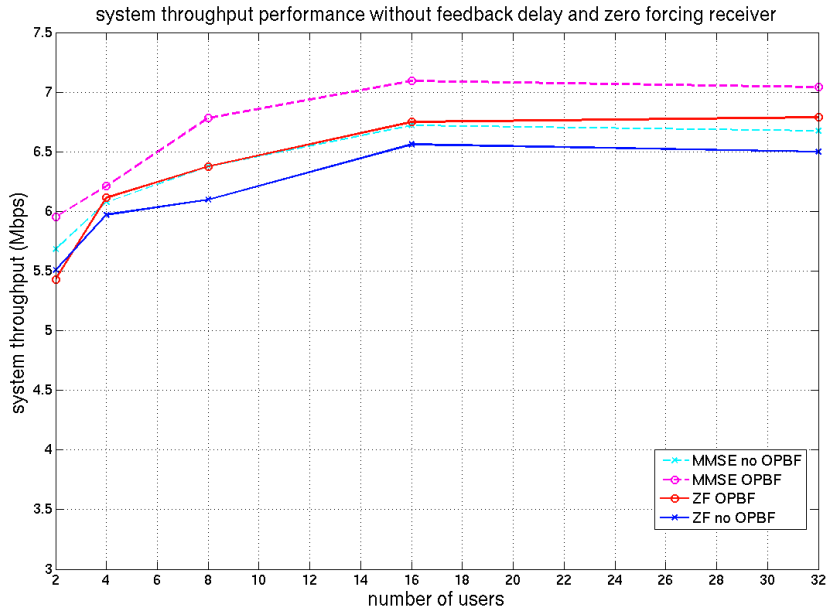

Figure A.2: Zero forcing and MMSE receiver performance with and without OPBF.

A.3 Effect of λ on MSE performance of RLS Estimator

In chapter 2.2.3 RLS filter forgetting factor λ was discussed. It was mentioned that $\lambda = 1$ corresponds to *infinite memory* and filter needs a forgetting factor to adapt itself to the new signal conditions if they change. Following figures show MSE performance of the filter under exactly the same conditions with only λ values changing in the system. ($\lambda = 1, \lambda = 0.99$ and $\lambda = 0.95$) Note that for $\lambda = 1$ we have the best performance and performance decreases as λ decreases. However as mentioned at the beginning of the paragraph, in real situations $\lambda = 1$ is not a good choice because signal statistics may change and infinite memory means the previous signal statistics will not be forgotton even if they are very different from the current statistics. So $\lambda < 1$ is a desirable constraint. Hence a λ value less than 1 but close to 1 is an ideal choice.

A.4 Exact Form of Gaussian Spatial Distribution

In chapter 2.4.3 Gaussian pad was discussed and a simpler approximation to the exact formula was given. Exact formula is as follows [24]:

$$p(\theta) = \frac{1}{2\pi} e^{-\frac{r_{MS}^2}{2\sigma_\theta^2}} + \frac{r_{MS}cos(\theta)}{\sigma_\theta\sqrt{8\pi}} e^{-\frac{r_{MS}^2 sin^2(\theta)}{2\sigma_\theta^2}} erfc\left(-\frac{r_{MS}cos(\theta)}{\sqrt{2}\sigma_\theta}\right), \qquad -\pi \leq \theta \leq \pi \quad \text{(A.1)}$$

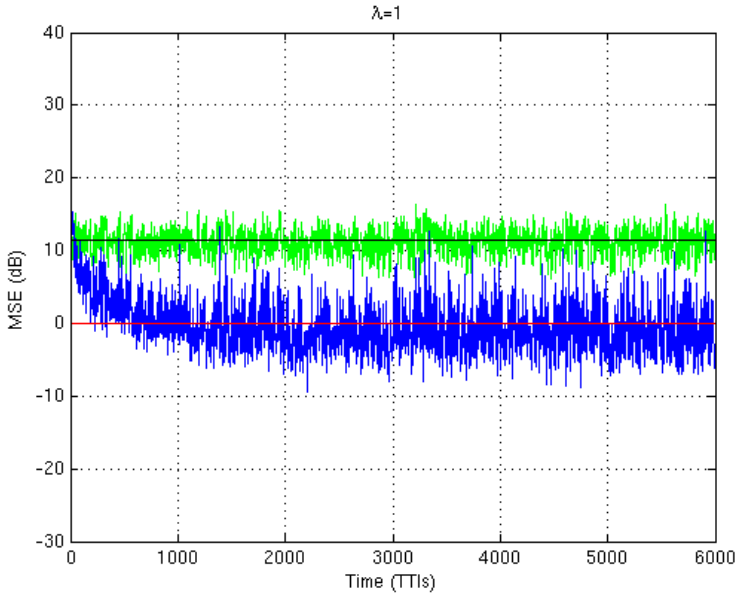

Figure A.3: MSE performance of the RLS estimator for forgetting factor $\lambda = 1$

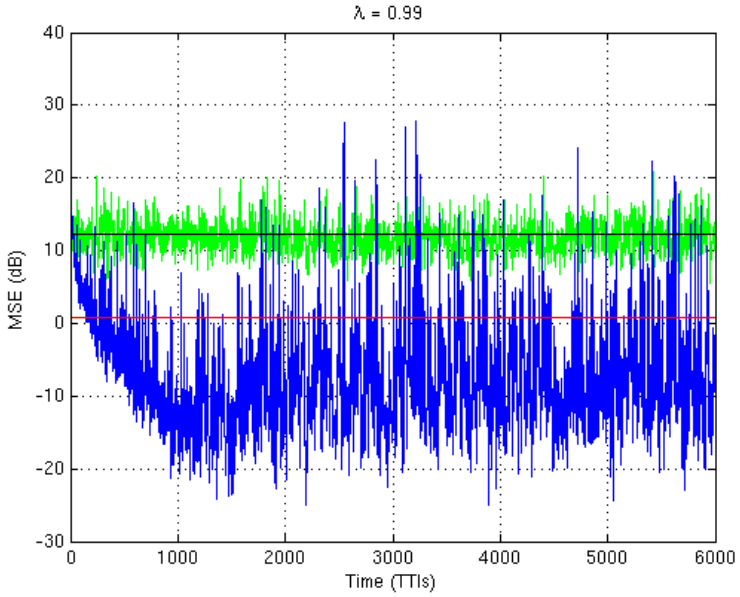

Figure A.4: MSE performance of the RLS estimator for forgetting factor $\lambda = 0.99$

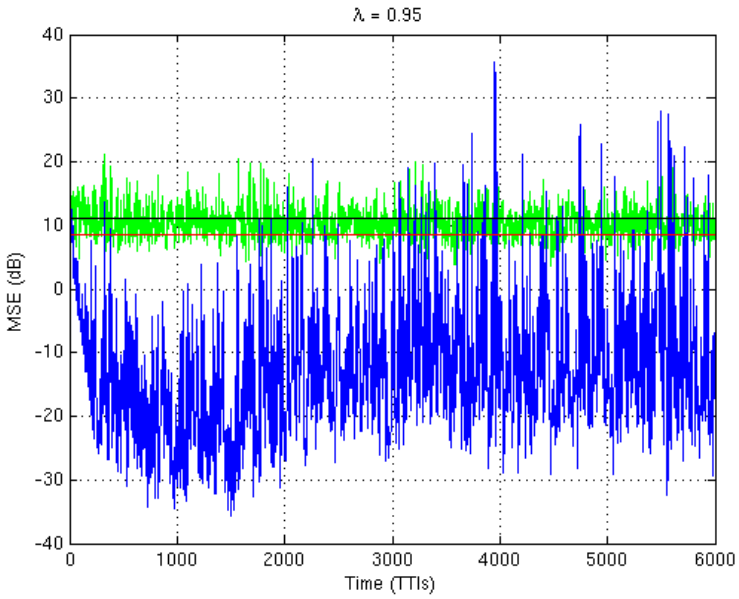

Figure A.5: MSE performance of the RLS estimator for forgetting factor $\lambda = 0.95$

List of Figures

List of Tables

Bibliography

[1] Pramod Viswanath, David N. C. Tse and Rajiv Laroia, "Opportunistic beamforming using dumb antennas," *IEEE Transactions on Information Theory*, vol. 48, June 2002.

[2] L. Dong, Teng Li, Y. Huang, "Opportunistic transmission scheduling for multiuser mimo systems," 2003.

[3] J. Chung, C Hwang, K. Kim, Y. Kyun Kim, "A random beamforming technique in mimo systems exploiting multiuser diversity," *IEEE Journal on selected areas in communications*, vol. 21, june 2003.

[4] R. Knopp and P. Humblet, "Information capacity and power control in single cell multiuser communications," in *Proc. IEEE Int. Computer Conf.*, June 1995.

[5] David Tse, Pramod Viswanath, *Fundamentals of Wireless Communication*. Cambridge University Press, 2005.

[6] H. Holma and A. Toskala, *WCDMA for UMTS*. John Wiley and Sons, Ltd, 2000.

[7] Hosein P. A., "Qos control for wcdma high speed packet data," *International Workshop on Mobile and Wireless Communications Networks, Stockholm, Sweden*, September 2002.

[8] I. E. Telatar, "Capacity of multi-antenna gaussian channels," *Eur. Trans. Telecom*, vol. 10, pp. 585–595, November 1999.

[9] J. Blanz, A. Klein and W. Mohr, "Measurement-based parameter adaptation of wideband spatial mobile radio chanel models," *In Proceedings of the IEEE International Symposium on Spread Spetrum Techniques and Applications, Mainz, Germany*, 1996.

[10] A. Klein and W. Mohr, "A statistical wideband mobile radio channel including the directions-of-arrival," *In Proceedings of the IEEE International Symposium on Spread Spetrum Techniques and Applications, Mainz, Germany*, 1996.

[11] K. I. Pedersen, P. E. Mogensen, and B. H. Fleury, "Power azimuth spectrum in outdoor environments," *Electronics Letters*, August 1997.

[12] K. I. Pedersen, P. E. Mogensen, and B. H. Fleury, "A stochastical model of the temporal and azimuthal dispersion seen at the base station in outdoor propagation environments," *IEEE Transactions on Vehicular Technology*, March 2000.

[13] Y. Lee, "Effects on correlation between two mobile radio base-station antennas," *IEEE Transactions on Communications*, 1973.

[14] U. Krause, "Design of opportunistic beamforming algorithms for highrate multiuser systems," Master's thesis, Institute for Integrated Signal Processing Systems, RWTH Aachen University, 2003.

[15] W. C. Jakes., *Microwave Mobile Communications*. John Wiley and Sons, New York, 1974.

[16] T. Fulghum, K. Molnar, and A. Duel-Hallen, "The jakes fading model for antenna arrays incorporating angular spread.technical report," *Center for Advanced Computing and Communication, North Carolina State University*.

[17] J. Salz and J. H. Winters, "Effect of fading correlation on adaptive arrays in digital mobile radio," *IEEE Transactions on Vehicular Technology*, November 1994.

[18] R. H. Clarke., "A statistical theory of mobile-radio reception. the bell system technical journal," p. 9571000, July-August 1968 1997.

[19] P. Petrus, J. H. Reed, and T. S. Rappaport, "Geometrical-based statistical macrocell channel model for mobile environments," *IEEE Transactions on Communications*, March 2002.

[20] R. B. Ertel and J. H. Reed., "Angle and time of arrival statistics for circular and eliptical scattering models," *IEEE Journal on Selected Areas in Communications*, November 1999.

[21] J. Fuhl, A. F. Molisch, and E. Bonek, "Unied channel model for mobile radio systems with smart antennas," *IEE Proc. Radar, Sonar Navig.*, February 1998.

[22] F. Adachi, M. T. Feeney, A. G. Williamson, and J. D. Parsons, "Crosscorrelations between the envelopes of 900 mhz signals received at a mobile radio base station site part f," *IEE Proceedings*, October 1986.

[23] M. P. Ltter and P. van Rooyen, "Modeling spatial aspects of cellular cdma/sdma systems," *IEEE Communications Letters*, May 1999.

[24] R. Janaswamy., "Angle and time of arrival statistics for the gaussian scatter density model," *IEEE Transactions on Wireless Communications*, July 2002.

[25] 3rd Generation Partnership Project, "Technical specification group radio access network; spatial channel model for multiple input multiple output (mimo) simulations (release 6)," Tech. Rep. v 6.1.0, 2003.

[26] J. P. Kermoal, L. Schumacher, K. I. Pedersen, P. E. Mogensen, F. Frederiksen, "A stochastic mimo radio channel model with experimental validation," *IEEE Journal on selected areas in communications*, vol. 20, August 2002.

[27] H. Kaarenen, A. Ahtiainen, L. Laitinen, S. Naghian, V. Niemi, *UMTS Networks - Architecture, Mobility and Services*. John Wiley and Sons, Ltd, 2001.

[28] "3gpp technical specification 25.212, multiplexing and channel coding," tech. rep., 2002.

[29] B.Zerlin, M.T. Ivrlac, W. Utschick, and J.A. Nossek, "Joint optimization of radio parameters in hsdpa," *IEEE Vehicular Technology Conference, Stockholm, Sweden.*, Spring 2005.